Circuit and Electromagnetic Design Notes

Note 53

1 April 2006

(Reprinted: Printing Errors in Previous Version.)

Scattered EM Field Responses of Canonical Scatterers Illuminated by an Impulse Radiating Antenna (IRA)

F. M. Tesche
Holcombe Dept. of Electrical and Computer Engineering
College of Engineering & Science, 337 Fluor Daniel Building
Box 340915, Clemson, SC 29634-0915

D. V. Giri
Pro-Tech, 11 C Orchard Court, Alamo, CA 94507-1541

and

W. D. Prather

Directed Energy Directorate, Air Force Research Laboratory, Kirtland AFB, NM 87117

Abstract

This note investigates the possibility of using the IRA as both a transmitter and receiver of electromagnetic fields for the purpose of target identification. Of specific interest is being able to estimate the induced open circuit voltage at the IRA source terminals when it is illuminated by a scattered EM field from simple conducting bodies excited by an incident field from the same IRA acting as a transmitter. In this study, several different canonical scatters are considered, including thin wires, spheres, conducting boxes, and an infinite conducting plate. For a 7 kV pulse excitation of the IRA, received peak transient voltages at the antenna range from a few volts to about 400 volts, depending on the scatterer.

Work conducted under the provisions of a Small Business Innovation Research (SBIR) Phase II contract FA9451-04-C-0150 awarded by the Directed Energy Directorate, Air Force Research Laboratory, Kirtland AFB, NM 87117 to Pro-Tech.

Contents

1. Introduction

In the 1960's, frequency-independent antennas were the rage. Log-periodic, spiral and conical-log spiral antennas were introduced by Rumsey and others, and Prof. R. DuHamel was investigating ways of feeding lens and reflector antennas in such a way that they could also operate over a large frequency range. In an early paper presented in an IEEE APS Symposium [1], DuHamel and his co-authors describe an innovative antenna design for this purpose. This antenna consisted of a paraboloidal reflector fed by several wires starting from the focal point, without any terminating resistors at the end of the wires Unfortunately, as far as one can tell from a literature search, this antenna design by DuHamel was never pursued and used in antenna applications.

In 1989 Baum independently conceived of a broad-band antenna concept, which he referred to as the "Impulse Radiating Antenna", or IRA [2]. This concept was developed for the purpose of being able to simulate transient EM fields at a target for a wide variety of applications – including defense and civilian applications.

Subsequent investigations into the radiating properties of the IRA [3] show that it is possible to design a reflector-style antenna that can operate in a phase coherent manner over several decades in frequency. Within the operating band of the IRA, the radiated field from the antenna is almost a linear function of frequency, implying that the radiated field in the time domain looks like the derivative of the applied transient voltage source driving the antenna. Hence, if a step function voltage were applied to the antenna, the radiated E-field at a distance would appear similar to a delta function in time[1].

Among the many applications of the IRA as a wideband radiator [4], its use as a *receiver* of wideband signals is intriguing. As may be noted from the reciprocity theorem (to be described in Section 2.5) within the operating band of the antenna, the received response is approximately proportional to the incident field on the antenna. In the time domain, this implies that the waveform of the induced response of the antenna (say the short-circuit current) is approximately proportional to the waveform of the incident field.

An interesting application of the IRA, therefore, is its possible use as both a transmitter of a fast pulse to interrogate a scatterer, and then its use as a receiver for detecting the backscattered signal, as suggested in Figure 1. In this note we examine this dual-use for the IRA and illustrate the levels of received open circuit voltage in the IRA for a number of different scattering bodies illuminated by the IRA.

---

[1] Of course, the step function response of the IRA would not be an exact impulse function. Because an antenna cannot radiate DC into the far field, any waveform produced from this antenna at a distant observation point must have zero area, which precludes the impulse function. The actual radiated field from the IRA for a step function excitation is reminiscent of the delta function, but has a zero net area. Thus, this transient waveform is referred to as being "impulse-like."

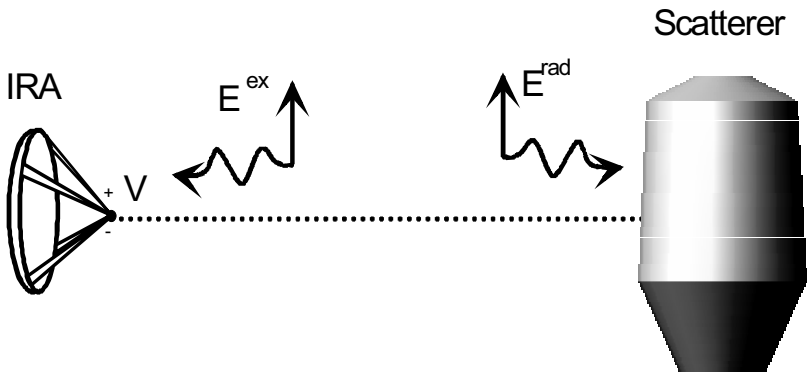

Figure 1. Illustration of the IRA illuminating a distant scatterer with field E^{rad}, and receiving a scattered field E^{ex}.

2. Theoretical Foundations

2.1 IRA Geometry

As described in an early paper by Baum [2] and later in [5, 6], the IRA consists of a parabolic reflector having a diameter D and focal length F. The antenna is fed by a parallel combination of two constant impedance conical transmission lines from an effective voltage source at the focal point. This geometry of this antenna and the feed structure are shown in Figure 2.

In this antenna there are two 400 Ω conical transmission lines that form feed-arms connecting the equivalent voltage source at the focus of the parabolic dish to the edge of the dish. Each feed arm is terminated in a resistance of 200 Ω at the dish edges (not shown in the diagram), and this provides a total of 400 Ω as a matched termination resistance at the ends of each of the two feed arm assemblies.

The specific IRA planned for the scattering measurement program is a modified version of a commercially available IRA from Farr Research. The modifications consist of:

i) changing the feed arms from $\pm$ 30 degrees to $\pm$ 45 degrees

ii) replacing the balun with SMA connector by a new balun with a HN connector to handle higher voltages and

iii) redesigning the termination section by a distributed termination of series / parallel connections of carbon composition resistors.

This is a parabolic dish antenna having dimensions D = 0.46 meters and F = 0.23 meters and resulting in a F/D ratio of 0.5. Due to the way that the pulser is connected to the feed arms through a balun, the total voltage exciting the feed arms across the dish is effectively *double* the pulser voltage V_o. This voltage V_o. is the output voltage from the pulser, when it is loaded by a 50 Ω resistance. Additional details of the feeding of the IRA are provided in ref. [7].

The EM field produced by the antenna is described in the coordinate system shown in Figure 2. At observation ranges sufficiently far from the antenna, the observation point is said to be in the "far field" of the antenna. Giri [8] has shown that for an IRA of diameter D, the range of the effective far-field in the time domain is given by

$$r \geq \frac{D^2}{2c\tau_r} \tag{1}$$

where τ_r is the rise time of the pulser source exciting the antenna. For a 0.48 meter antenna and a pulser with a rise time of about 100 ps, which is the nominal rise time of typical solid-state pulsers, (e.g., FID technology, Kentech etc.), the far-field occurs for $r > 3.5$ meters. Of course,

for observation points closer than 3.5 meters, there *is* a strong transient EM field produced, but it contains a radial as well as transverse field components. The EM field produced by the antenna in this range does not appear as a simple plane wave.

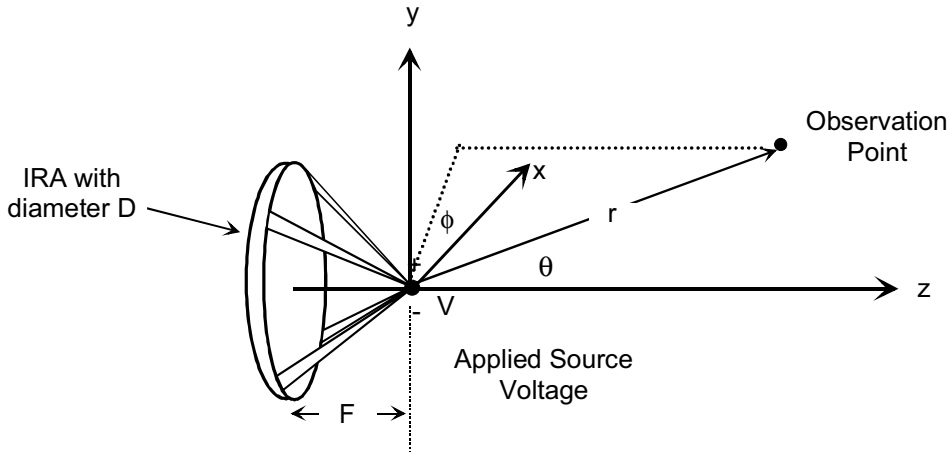

Figure 2. Geometry of the IRA, showing the coordinate system and a distant field observation point.

2.2 Antenna Excitation Source

The pulser that is planned for the experimental work is a PBG 1 high-voltage pulse source built by Kentech Instruments Ltd. The peak amplitude is typically 7 kV into a 50 Ω load, and the output waveform consists of a fast rising edge followed by an exponential decay. The full-width to half-max (FWHM) time of the pulse is about 3 ns and the 10-90% rise time is about 100 ps. The pulser has an internal repetition rate and delay generators, as well as an amplitude control.

To use this waveform for an analysis of the EM fields produced by the IRA, we use a smooth analytical fit to the overall pulse shape. According to Giri [9], a reasonable representation of such a pulse is given by the expression

$$\mathrm{V_o}(t) = \mathrm{V}_p\left(1+\Gamma\right)e^{-\left(\frac{t-t_s}{t_f}\right)}\left[0.5\ \mathrm{erfc}\left(-\sqrt{\pi}\,\frac{t-t_s}{t_r}\right)\mathrm{u}\left(-(t-t_s)\right)+\left[1-0.5\ \mathrm{erfc}\left(\sqrt{\pi}\,\frac{t-t_s}{t_r}\right)\right]\mathrm{u}\left(t-t_s\right)\right] \quad (2)$$

where *erfc* (.) denotes the complementary error function and *u*(.) is the unit step (Heaviside) function. Using this equation, it is found that the following parameters provide a good fit to the PBG 1 pulser waveform:

V_p = 7 (kV) – peak value of waveform

Γ = 0.02 – amplitude adjustment parameter

τ_r = 100 (ps) – waveform rise parameter

τ_f = 4.255 (ns) – waveform decay parameter

τ_s = 0.1 (ns) – time shift for t = 0

Figure 3 shows the resulting analytical pulser waveform, as given by Eq.(2), and this waveform will be the excitation for all transient calculations in this report.

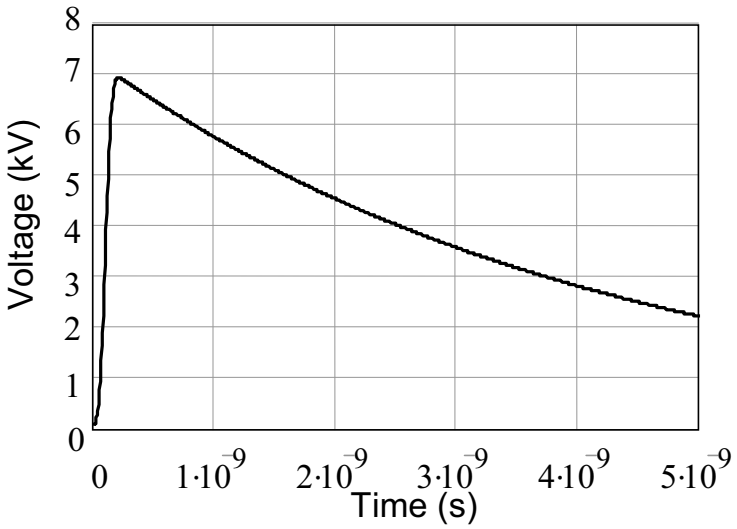

Figure 3. Analytical representation of the PBG-1 pulser waveform as provided by Eq.(2) with a risetime of 100 ps and FWHM = 3 ns.

The frequency domain spectrum of the waveform in Eq.(2) can be expressed analytically as

$$\tilde{V}_o(\omega) = \frac{V_p(1+\Gamma)t_f}{(1+j\omega t_f)} e^{(1/4\pi)\left(\frac{t_r}{t_f}+j\omega t_r\right)^2} \quad \text{(Volts / Hz)} \ . \qquad (3)$$

A plot of the magnitude of this spectrum is provided in Figure 4. Note that this excitation has significant spectral components to about 4 GHz.

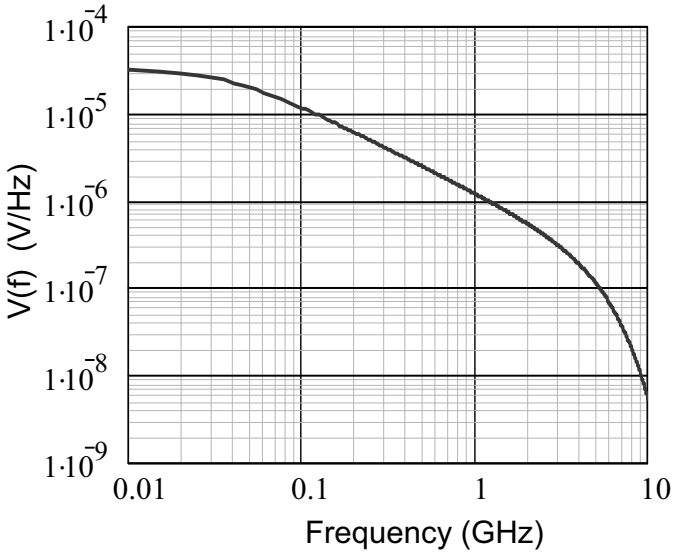

Figure 4. Plot of the spectral magnitude of the excitation voltage waveshape of Figure 3.

2.3 Determination of the Radiated EM Fields

A recent Russian paper [10] has developed an analytical expression for the near- and far-field transient E-field produced by an IRA fed by a two-arm feed structure, as shown in Figure 5. The advantage of this analysis is that the transient E-field is given directly in terms of the antenna geometry and the transient pulser voltage waveform without the need for Fourier transforms applied to an antenna spectral response. In addition, the Russian results are valid for both on-axis and off-axis observation locations, as long as the observation point lies within a cylindrical region extending from the dish edge in the boresight direction.

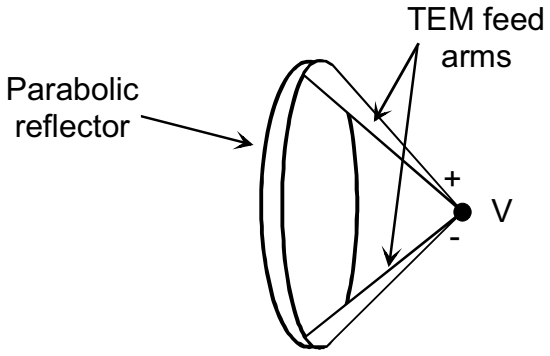

Figure 5. Illustration of the radiation mechanisms in an IRA fed by a two-arm transmission line.

For the IRA having a dish diameter D, focal length F, feed arm length L and feed arm angle β as shown in Figure 6, reference [10] provides the expression for the on-axis transient E_y field component as

$$E_z(r;t) = \frac{1}{2\pi f_g}\left\{\left[\frac{V(t-r/c)}{r}\frac{\sin\beta}{1+\cos\beta} - \frac{V(t-L/c-r_2/c)}{r_2}\frac{\sin\beta+\sin\gamma}{1+\cos(\beta-\gamma)}\right]\right\} \\ -\left[\frac{4V(t-2F/c-r/c)}{D} - (2+2\cos\gamma)\frac{V(t-L/c-r_2/c)}{D}\right] \quad (4)$$

In this equation, r is the distance from the source feed of the antenna to the on-axis observation point, γ and r_2 are the angle and distance, respectively, from the antenna dish edge to the observation point, and V (t) is the transient voltage applied across the feed arms of the antenna. The term $f_g = Z_f / Z_c$, where Z_f is the characteristic impedance of the feed arm structure (typically 400 Ω) and $Z_c = 120\pi$ is the free-space wave impedance. Thus, for this antenna, $f_g = 1.06$.

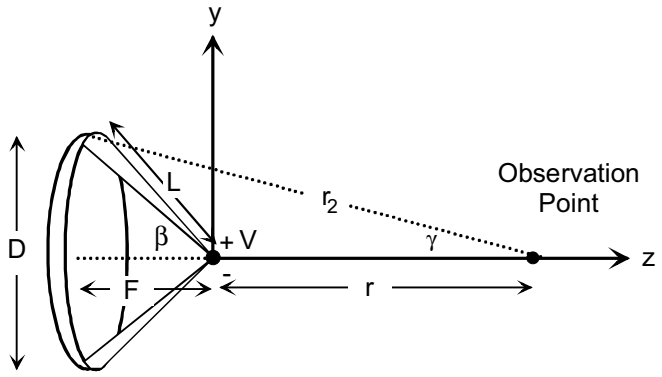

Figure 6. Geometry of the two-arm IRA with pertinent parameters for computing the on-axis field.

The actual antenna to be used in the scattering measurements is a variation of the two-arm antenna of Figure 6, in that it has a four arm feed. This feed consists of two 400 Ω feed arms in parallel, each rotated approximately 45 degrees relative to the position shown in Figure 6. The resulting feed structure is shown in Figure 7 and the parallel combination of these feed arms presents an input impedance of 200 Ω at the effective feed source at the focal point of the reflector.

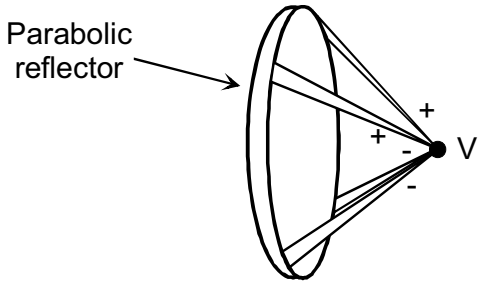

Figure 7. The IRA excited by a four-arm feed structure.

The radiated field for the four arm IRA may be calculated from the two arm result by multiplying Eq.(4) by a factor of $\sqrt{2}$, which is simply the vector sum of the fields from a pair of orthogonal feeds [11]. This accounts both for the presence of the two separate feed arm pairs and the fact that they are rotated spatially. In doing so it must be recalled that the transient voltage $V(t)$ in Eq.(4) is the *applied* voltage across the dish reflector.

The pulser source has an unbalanced coaxial output and produces an output voltage $V_o(t)$ in a 50 Ω load,. To connect this 50 Ω source to the balanced 200 Ω input of the IRA, a 20 Ω to 200 Ω balun is used. As shown in Figure 8, this balun consists of two 100 Ω coaxial cables connected in parallel at the pulser end and in series at the IRA feed end. With this balun, the effective driving voltage placed across the IRA feed arms is twice the pulser voltage: $V(t) = 2\ V_o(t)$. Reference [7] provides additional information on the design and operation of this type of balun.

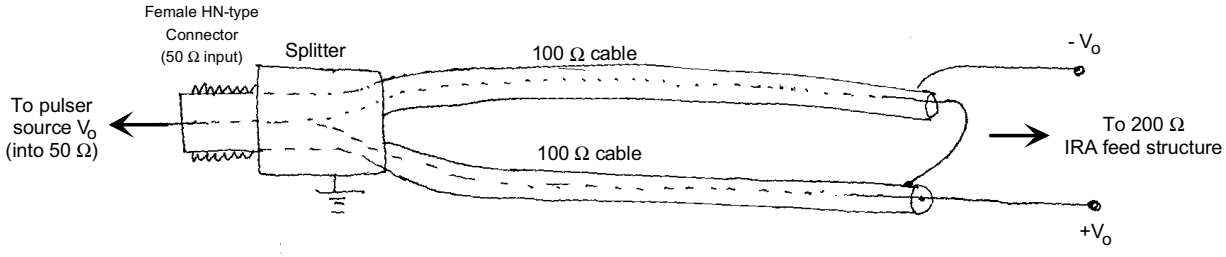

Figure 8. Details of the 50 Ω to 200 Ω balun connecting the pulser source to the IRA feed structure.

For the IRA with four feed arms and the balun feed, the on-axis E-field produced by the applied pulser excitation is given from Eq.(4) with appropriate factors of 2 and $\sqrt{2}$ included as

$$E_z(r;t) = \frac{\sqrt{2}}{\pi f_g}\left\{\left[\frac{V_o(t-r/c)}{r}\frac{\sin\beta}{1+\cos\beta} - \frac{V_o(t-L/c-r_2/c)}{r_2}\frac{\sin\beta+\sin\gamma}{1+\cos(\beta-\gamma)}\right]\right. \\ \left. -\left[\frac{4V_o(t-2F/c-r/c)}{D} - (2+2\cos\gamma)\frac{V_o(t-L/c-r_2/c)}{D}\right]\right\}. \qquad (5)$$

2.4 IRA Radiated Fields

2.4.1 Transient Responses

For the pulser excitation of Figure 3, the transient, on-axis E-field for the 0.4699 meter diameter IRA has been calculated using Eq.(5). Figure 9a and 9b present the transient E-field responses at different ranges. Note that the range r is defined at the distance from the IRA source feed to the field observation point, as shown in Figure 2. In this case, the angle $\theta = 0^o$, as the observation point lies along the z axis.

It is noted that far from the antenna, the E-field amplitude is decreasing as 1/r. Figure 10 plots the maximum E-field arising from the impulse-like peak as a function of range. In this plot it is evident that for distances greater that about 3 or 4 meters, the fields do indeed have a 1/r fall off.

Another indicator of the antenna performance is to compute the transient "far-field gain" of the antenna, defined as the peak value of $rE_y(t)/V_o$, where again, V_o is the peak value of the applied pulser voltage. This quantity has been calculated for the IRA, and the plot of this gain parameter is shown in Figure 11.

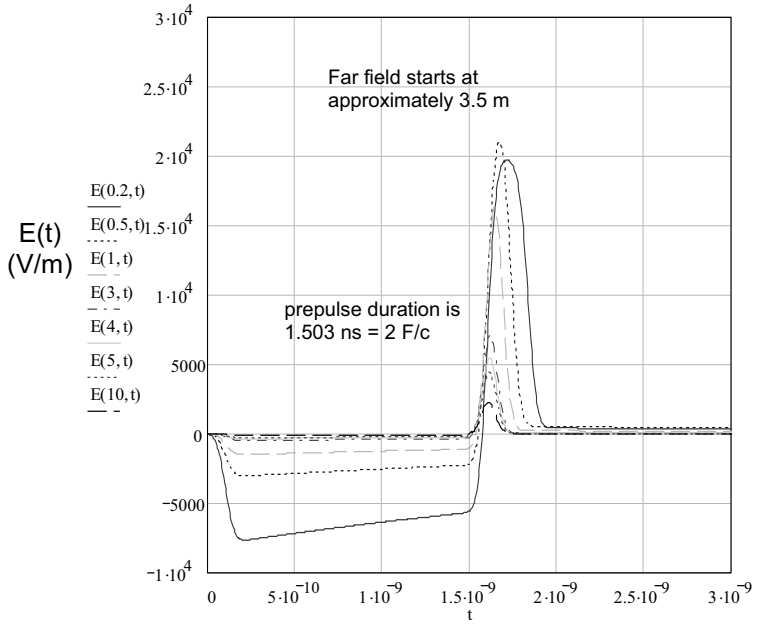

(a) Detailed E-fields as a function of retarded time

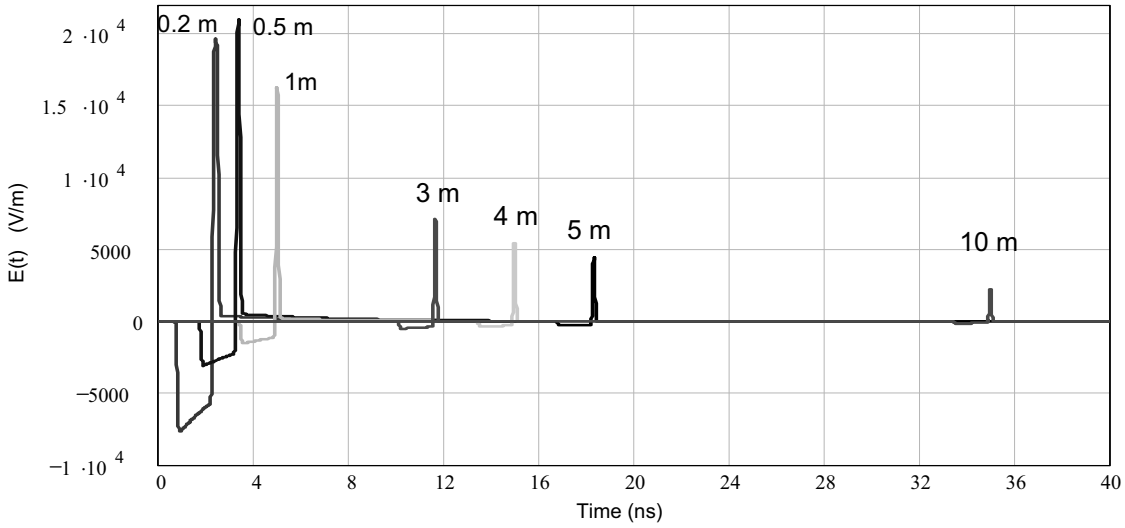

(b) Temporal boresight fields

Figure 9. Plots of the on-axis transient E-field for different ranges *r* from the antenna.

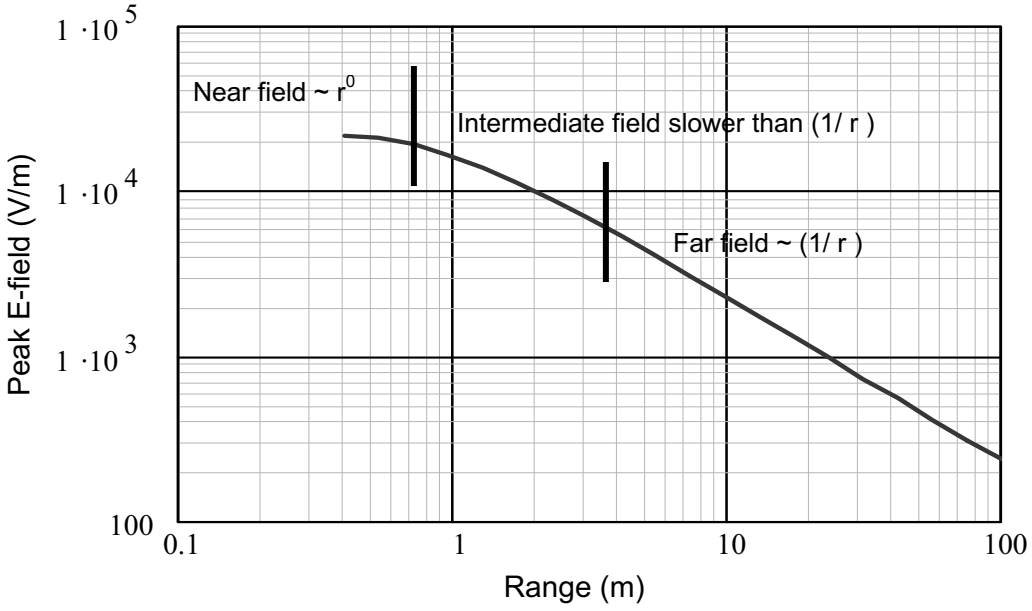

Figure 10. Plot of the peak E-field as a function of range *r* from the IRA.

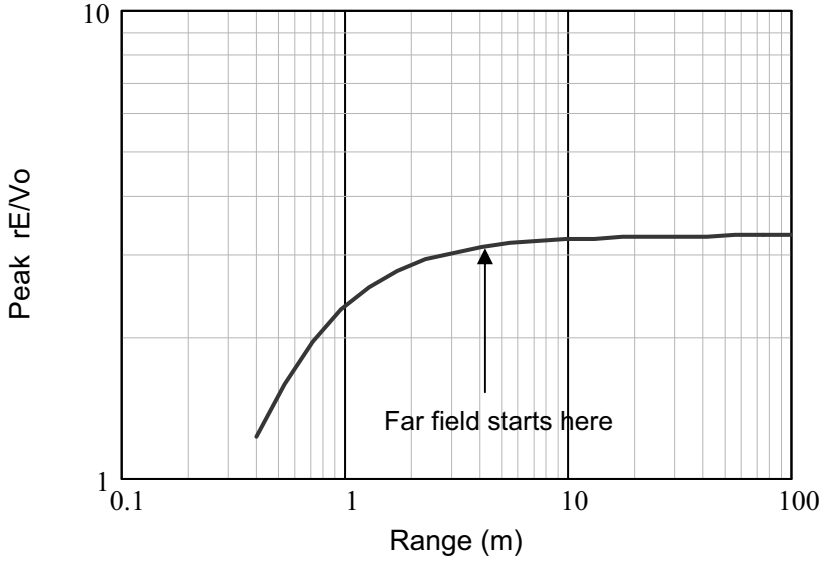

Figure 11. Plot of the peak normalized E-field rE/V_o as a function of range *r* from the IRA.

In ref [8] there are closed form and simple expressions for the peak prepulse and peak impulsive waveform amplitudes. For the peak prepulse we have (from Eq. 5.38 of [8])

Prepulse: $$E_{peak} \approx \frac{2V_o}{r}\frac{D}{4\pi f_g}\frac{1}{2F}\sqrt{2} \quad \text{(V/m)} \qquad \text{(Valid for all r)} \qquad (6)$$

and the peak impulse (from Eq. 5.39 of [8]) is given by

Impulse: $$E_{peak} \approx \frac{1}{r}\frac{D}{4\pi c f_g}\, 2\sqrt{2}\, \left.\frac{\partial V_o}{\partial t}\right|_{peak} \text{(V/m)} \quad \text{(Valid in the far field)} \qquad (7a)$$

leading to

$$\frac{r\,E^{rad}(r,f)}{V_o(f)} \approx j\omega\,\frac{D\,2\sqrt{2}}{4\pi c\, f_g} \quad \text{(Valid in the far field)} \qquad (7b)$$

In these expressions, recall that $2V_o$ is the peak voltage applied across the IRA dish (twice the peak pulser voltage, due to the voltage doubling effect of the balun), $\partial V_o/\partial t\,|_{\text{peak}}$ is the peak rate of rise of the pulser source voltage and r is the distance between the IRA and the field observation point. The parameters D, F and f_g have been defined previously.

Applying Eq.(6) to the specific IRA geometry under consideration here for an observation point at a distance of r = 4 meters yields a prepulse amplitude of 387 V/m, while the transient analysis shown in Figure 9 provides a prepulse of 383 V/m – about a 1% difference. Similarly, at the same distance Eq.(7) provides a peak impulse E-field of 5815 V/m, while the present analysis yields 5424 V/m. This amounts to about a 6.7 % difference[2].

2.4.2 Spectral Responses

Taking the Fourier transform of the waveforms of the on-axis fields in Figure 9 yields the spectral responses of the waveforms, which are denoted as $E^{rad}(f)$. Figure 12 presents the plots of these spectra as a function of frequency for different ranges from the IRA.

Also of interest is the antenna transfer function that relates the radiated E-field spectrum at a distant point to the spectrum of the pulser excitation. For convenience, this transfer function can be normalized by the range r and the phase function relating to the

---

[2] It should be pointed out that these calculations use an idealized rate of rise of the pulser voltage, dV_o/dt., which is estimated from the pulser waveshape as applied to a 50 Ω load. In the physical IRA, the fast rising pulser waveform is applied to the balun, and the rise time of the output voltage that is ultimately launched onto the IRA reflector is degraded. Consequently, it is estimated that the actual IRA peak E-field levels could be about 50% of those calculated here with the unperturbed pulser risetime.

propagation time from the IRA source to the observation location. It is defined by the unit-less function $T_{IRA}(r, f)$ as

$$\begin{aligned} T_{IRA}(r,f) &= \frac{r\,E^{rad}(r,f)}{V_o(f)}\,e^{jkr} \\ &\approx \frac{j\omega D\,2\sqrt{2}}{4\pi c f_g}\,e^{jkr} \quad (\textit{Valid in the farfield}) \end{aligned} \tag{8}$$

where $k = 2\pi f/c$ is the wave propagation constant in free space.

Figure 13 presents a plot of the magnitude of this transfer function. Most notable is the fact that the overall behavior of the function is approximately proportional to frequency in the far field, which suggests that the radiated field appears like the derivative of the applied voltage. That this behavior is correct can be verified both analytically and numerically. This transfer function will be useful not only in calculating the radiated field from the IRA for arbitrary excitations, but also in computing the received signal from the IRA, as will be discussed in Section 2.5.

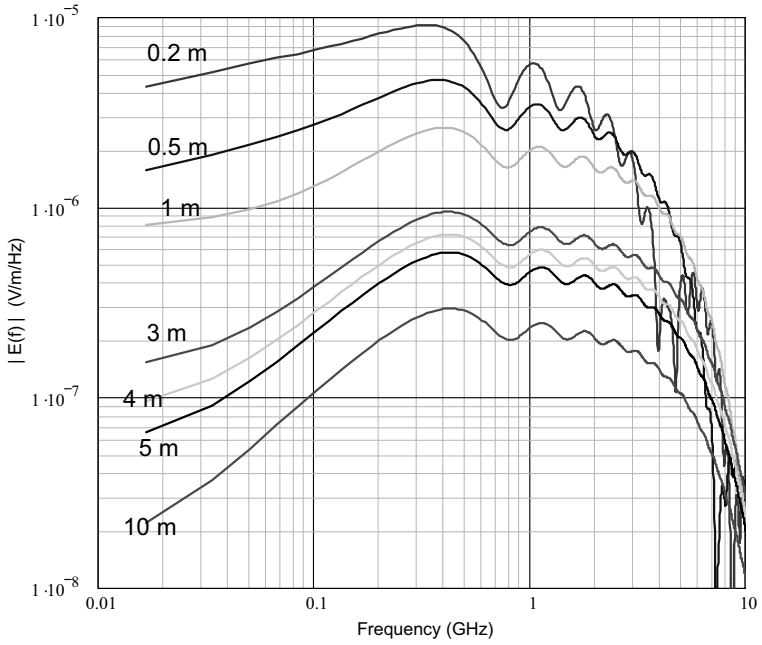

Figure 12. Plots of the spectral magnitudes $|E^{rad}(f)|$ for the on-axis radiated field, shown as a function of frequency for different ranges from the IRA.

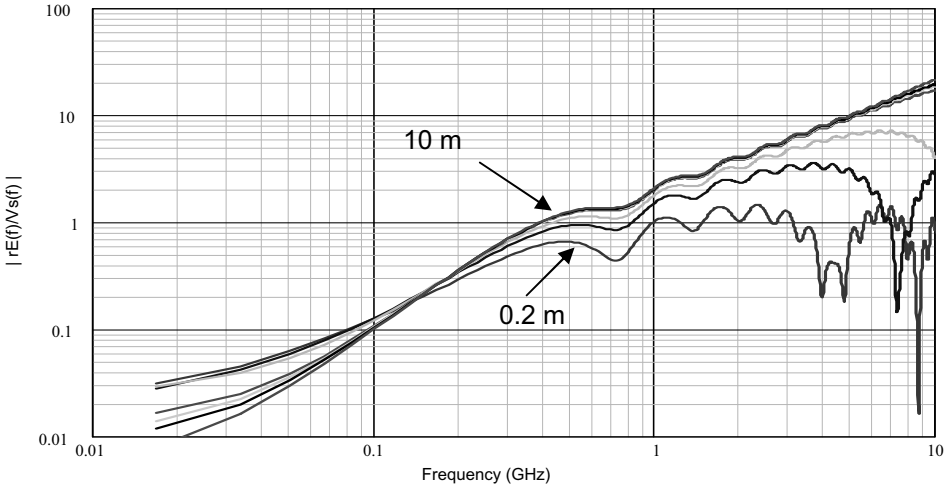

Figure 13. Plots of the transfer function magnitudes $|T_{IRA}| = |rE^{rad}(f)/V_o(f)|$ for the on-axis field for different ranges from the IRA

2.4.3 Spatial Extent of the Radiated IRA Fields

As the goal of this work is to estimate the received signal from the IRA, when it is used to illuminate a distant scattering body, it is important to understand the spatial behavior of the radiated IRA field in the vicinity of a potential scatterer. As the simplest scattering calculations assume an incident plane wave excitation, if the spatial behavior of the IRA field differs significantly from a plane wave, then a more complicated, non-plane wave scattering model must be developed.

To investigate this issue, the transient E-field in a 4m × 4m plane at a range of 4 meters was calculated, and the peak value extracted from the transient field. The geometrical configuration for this calculation is shown in Figure 14.

As the physical extent of the observation plane is larger than the range of validity of the off-axis computational model of [10], an alternate off-axis model has been used. This model is described in ref. [12] and involves determining the EM field distribution in the parabolic reflector aperture and then integrating over this aperture distribution to determine the radiated field. In addition, the radiation contributions from the currents flowing on the feed arms are included, thereby providing the pre-pulse contribution to the radiation. A comparison of the results from this aperture integration model with those from [10] shows excellent agreement.

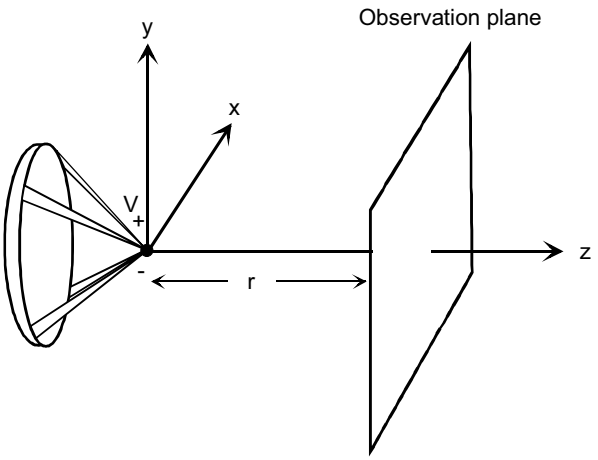

Figure 14. Illustration of the IRA antenna and a field observation plane at a distance *r* = 4 m.

Figure 15 presents surface and contour plots of the peak radiated E-field from the IRA as fed by the Kentech PBG 1 pulser. For this calculation the peak pulser voltage was ½ the normal pulser level (e.g., V_o = 3.5 kV instead of 7 kV). As a consequence, the peak value of the field along the boresight direction is about 2.7 kV/m, instead of the 5.4 kV/m shown in the transient response in Figure 9.

The contours in Figure 15 are in 5% increments of the peak value. The innermost circular region in the contour plot represents the spatial area where the incident IRA fields are approximately constant (within 5%). As a consequence, the incident IRA field in this region can be considered reasonably planar. This region is roughly a circle with a radius of about 20 cm. Any scattering object that fits into this region can be considered as being illuminated by a plane wave from the IRA.

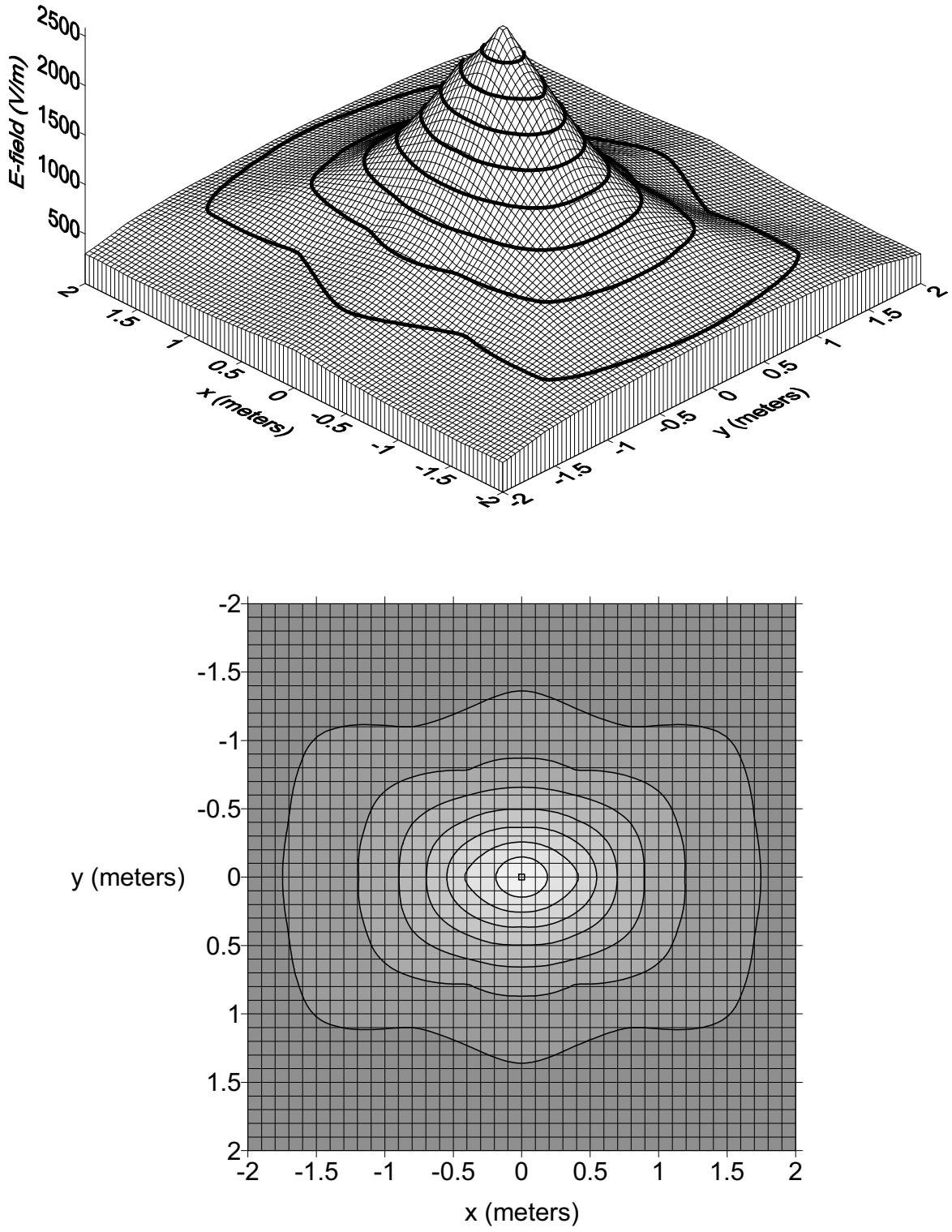

Figure 15. Plot of the peak E-field amplitude for the IRA at a distance of 4 meters. (Note that for this calculation, the peak pulser voltage was ½ the nominal value of 7 kV (e.g., V_o = 3.5 kV.)

2.5 IRA Operating in the Reception Mode

For the case of reception of EM signals by the IRA, it is convenient to consider the problem in the frequency domain, rather than directly in the time domain as was done for the radiation problem in Section 2.4.

The approach for determining the reception property of the IRA is to use the reciprocity theorem [13] which relates the transmitting properties of the antenna to the reception properties. In doing this, the antenna transmission or reception problem is regarded as a linear two port network, as shown in Figure 16. In this representation, port **a** represents the driving terminals of the antenna (e.g., the excitation point between the transmission line arms feeding the antenna) and port **b** denotes a far-field observation point where the scattering body is located.

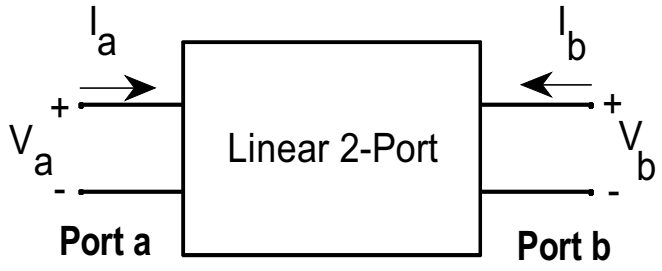

Figure 16. Representation of the antenna as a linear two-port network.

For this two port network, one can envision two separate cases involving different excitations or loads applied to terminals. Case 1 has terminal parameters V_{a1}, V_{b1}, I_{a1} and I_{b1} and case 2 has parameters V_{a2}, V_{b2}, I_{a2} and I_{b2}. Then, according to the reciprocity theorem, these parameters are related by the expression

$$V_{a1}I_{a2} + V_{b1}I_{b2} = V_{a2}I_{a1} + V_{b2}I_{b1} \tag{9}$$

where *a* and *b* denote the two ports of the network, and 1 and 2 refer to the different source configurations.

Various versions of Eq.(9) can be useful in special cases of the two-port excitation. Consider the source configurations shown in Figure 17 with $I_{b1} = 0$ in case 1 and $V_{a2} = 0$ in case 2. In this case, the reciprocity relation in Eq.(9) becomes

$$\frac{V_{b1}}{V_{a1}} = -\frac{I_{a2}}{I_{b2}}. \tag{10}$$

This last equation forms the basis for computing the reception properties of the IRA. Case 1 is the antenna transmission case, where a voltage source $V_{a1} = V_o(f)$ is applied to the

antenna, and a far-field voltage V_{b1} is detected at the observation point. Note as this voltage is an open-circuit quantity, $I_{b1} = 0$ as required. This voltage is defined as

$$V_{b1} = -E^{rad} d\ell \,, \tag{11a}$$

And upon substituting E^{rad} from Eq(8), V_{b1} may be expressed in terms of the antenna radiation transfer function T_{IRA} as

$$V_{b1} = -\frac{T_{IRA}}{r} e^{-jkr} V_o(f)\, d\ell \,, \tag{11b}$$

Case 2 represents the antenna reception problem, in which a distant current source I_{b2} radiates an EM wave towards the antenna and ultimately a short-circuit current $I_{sc} = I_{a2}$ is induced in the antenna terminals. Because the terminal ***a*** is short circuited, $V_{a2} = 0$ as previously noted. The goal in this use of the reciprocity theorem is to determine I_{sc}.

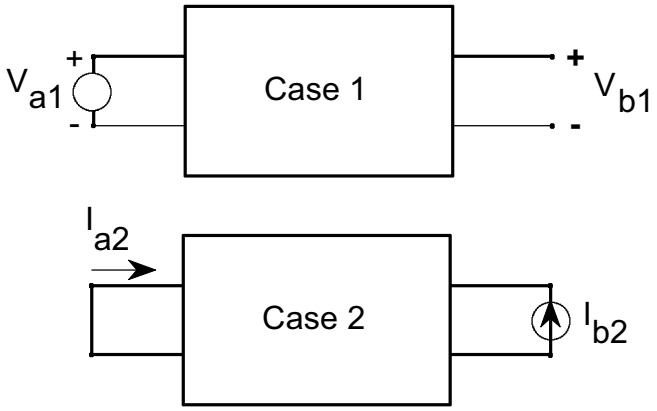

Figure 17. Application of the reciprocity theorem to the transmitting antenna (Case 1) and the receiving antenna (Case 2).

With Eq.(11b) substituted into Eq(10) the reciprocity relationship becomes

$$\frac{\frac{T_{IRA}}{r} e^{-jkr} V_o(f)\, d\ell}{V_o(f)} = \frac{I_{sc}}{I_{b2}} \,, \tag{12}$$

and upon solving for the desired short circuit current and clearing terms, we have

$$I_{sc} = T_{IRA} \frac{e^{-jkr}}{r} I_{b2}\, d\ell \tag{13}$$

Normally, we wish to relate the induced short-circuit current in the reception case to an incident EM field E^{ex} exciting the IRA, instead of to the current element strength in the far field, $I_{b2}\, d\ell$. To do this, we recall the expression for the E-field radiated by a point dipole moment $I\, d\ell$ from ref.[14] as

$$E^{ex} = jkZ_o\, Id\ell\, \frac{e^{-jkr}}{4\pi r} \quad = \quad j\omega \frac{Z_o}{c}\, Id\ell\, \frac{e^{-jkr}}{4\pi r} \quad = \quad j\omega\mu_o\, Id\ell\, \frac{e^{-jkr}}{4\pi r} \tag{14}$$

where μ_o is the free space permeability. Substituting into Eq.(13) the quantity $Id\ell$ expressed in terms of the excitation E-field from Eq.(14) gives the desired expression for the short-circuit current as a function of the incident E-field on the IRA:

$$I_{sc} \;=\; \frac{4\pi}{j\omega\mu_o}\, T_{IRA}\; E^{ex} \;. \tag{15}$$

In some cases, the open-circuit voltage induced in the antenna is of interest, especially if the antenna response is to be measured with a high impedance measurement device. In this case, we can perform a Norton to Thevenin transformation of the induced antenna current response to obtain the open circuit voltage as

$$V_{oc} \;=\; I_{sc}\, Z_{in} \;=\; \frac{4\pi}{j\omega\mu_o}\, Z_{in}\, T_{IRA} E^{ex} \;=\; h_{eq}\, E^{ex} \tag{16}$$

Here, Z_{in} is the input impedance of the antenna, as seen at its open circuit terminals. For the present IRA, this impedance is approximately 50 Ω.

Equation (16) serves to define the equivalent height of the antenna:

$$h_{eq} = \frac{4\pi}{j\omega\mu_o} Z_{in} T_{IRA} \;=\; \frac{4\pi}{j\omega\mu_o} Z_{in}\, \frac{rE^{rad}(r,f)}{V_o(f)}\;\; e^{jkr} \;= \frac{4\pi c}{j\omega}\left(\frac{Z_{in}}{Z_o}\right) \frac{rE^{rad}(r,f)}{V_o(f)} \tag{17}$$

Using the computed antenna transfer functions T_{IRA} shown in Figure 13, the equivalent heights of the IRA as a function of frequency for different locations of the source producing the incident field are shown in Figure 18.

Note that for the sources located closer than about 3 meters (in the near field) the equivalent height varies with the source position. For more distant sources, the incident excitation E-field is nearly planar and the equivalent heights are essentially independent of the position of the excitation source. For distant sources, the equivalent height of this particular IRA is seen to be roughly a constant 0.16 meters, from 200 MHz to well over 1 GHz.

When the scattering object is a distant source, one can use the far field approximation given in Eq.(7b) in Eq.(17), which leads to

$$h_{eq} \approx \frac{Z_{in}}{Z_o f_g} \; D \; 2\sqrt{2} \quad \approx \frac{50}{400} \; (0.46) \; x \; 2\sqrt{2} \cong 16 cm \, .$$

This is in agreement with the numerically computed value in Figure 18.

The fact that this function is similar to a constant for a very wide frequency range suggests that the received open circuit voltage waveform will be very similar to the waveform of the excitation E-field on the antenna.

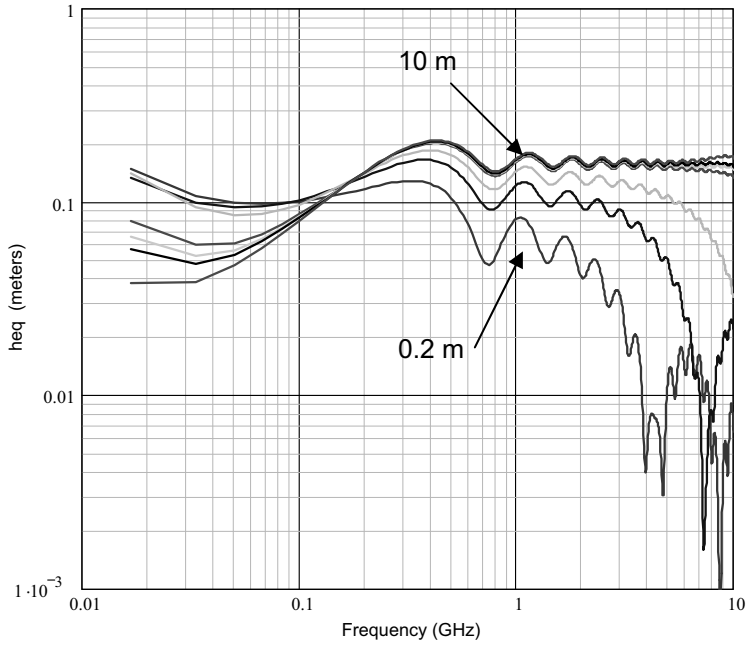

Figure 18. Plot of the equivalent height of the IRA as a function of frequency for different locations of the source producing the incident field.

2.6 EM Scattering by Distant Objects

We now express the excitation E-field at the IRA in the reception problem to the voltage excitation source for the antenna operating in the transmit mode. As noted in Figure 2, when the distant scatterer is illuminated by the incident field produced by the IRA, a portion of this signal is reflected and propagates back to the IRA. The strength of this reflected signal depends on the shape and orientation of the scatterer and also is a function of frequency. For a linearly polarized (E_y) incident field, the y-component of the reflected field can be described by a *scattering coefficient* $\Gamma(r, f)$ as

$$E_y^{ex} = \Gamma(r, f) \, E_y^{rad} \tag{18}$$

In this equation, E^{rad} is the IRA-radiated E-field at the scattering body and E^{ex} is the scattered field evaluated back at the IRA which serves to excite the antenna in its receiving

mode. As a consequence, the coefficient Γ is expected to have a e^{-jkr}/r functional dependence on the range.

Determination of Γ can be a complicated process and usually it involves numerical methods, the choice of which depends on the type of scatterer involved. Possible numerical solutions include the use of the electric field integral equation (EFIE), the magnetic field integral equation (HFIE), finite difference time domain (FDTD), and various analytic solutions. Additional information about these solution methods will be presented in the next section containing examples of IRA scattering responses.

With the scattered field defined via Eq.(18), the end to end expression relating the received open-circuit voltage to the pulser excitation can be developed. Substituting (18) into Eq.(16) and making use of the fact that $E^{rad}(f) = T_{IRA}\frac{e^{-jkr}}{r}V_o(f)$ from Eq.(8), we obtain the final expression for the spectrum of the open circuit voltage of the IRA:

$$V_{oc}(f) = \frac{4\pi}{j\omega\mu_o} Z_{in}\, T_{IRA}\, \Gamma(r,f)\, T_{IRA}\, \frac{e^{-jkr}}{r}\, V_o(f) \qquad (19)$$

Given the spectrum of the pulser voltage in Figure 4, the IRA radiated transfer function plotted in Figure 13 and the calculated scattering parameter Γ, the open circuit voltage spectrum may be evaluated with the above equation. The transient response may then be computed by an inverse Fourier transform.

3. Illustration of Computed Scattering Responses

In this section, a number of different scattering objects are considered for illumination and subsequent reception of the backscattered signal from the 0.47 meter IRA. The scatterer is located in the boresight direction of the IRA at a distance of 4 meters from the IRA feed-arm apex to the center of the scattering body (See Figure 1). We intend to perform the measurements at this scatterer / target distance of 4m for the canonical scatterers considered in this section. As noted in Section 2.4.3 the physical extent of the scatterer is constrained to lie within a region having a radius of about 20 cm for the incident field from the IRA to be approximately planar.

The radiated E-field from the IRA illuminating the various scatterers is the field calculated for a range r = 4 meters, as shown in Figure 9. This waveform, which is referred to as E^{rad} in this document, is reproduced on a more convenient scale in Figure 19 below.

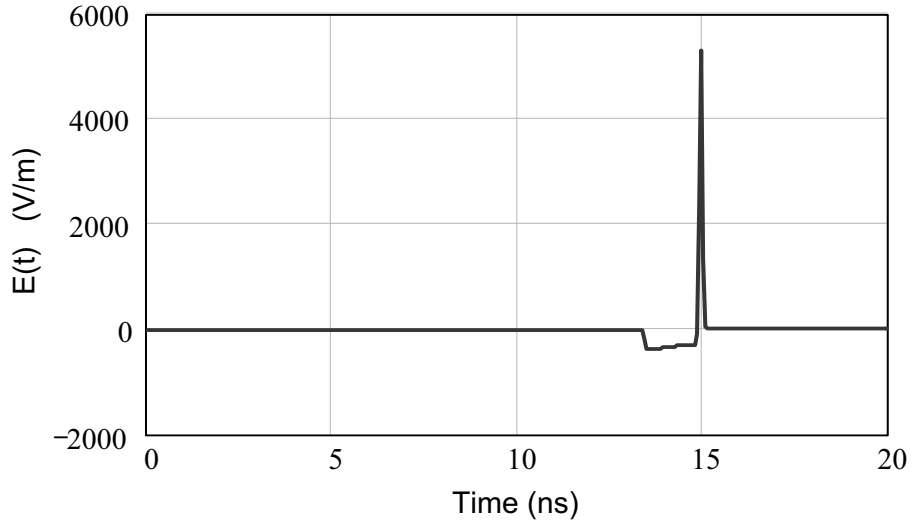

Figure 19. Radiated E-field E^{rad} at a distance of r = 4 meters used for all scattering calculations.

The corresponding spectral amplitude for this waveform (shown previously in Figure 12) is presented here in Figure 20, and the field transfer function magnitude $|T_{IRA}| = |rE^{rad}(f)/V_o(f)|$ needed for the scattering calculations in Eq.(19) is given in Figure 21. Of course, when Eq.(19) is evaluated, the entire complex-valued transfer function is used, not just the magnitude.

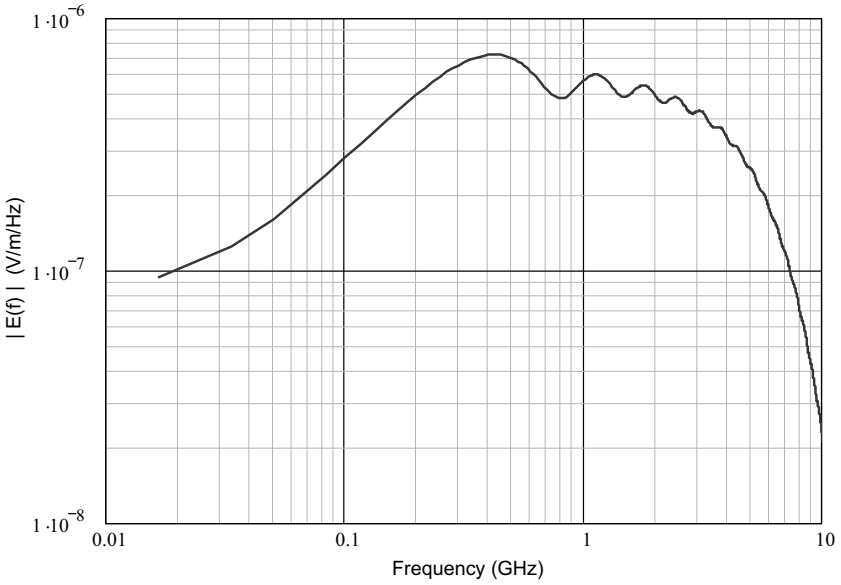

Figure 20. Spectral magnitude of the radiated E-field E^{rad} at a distance of r = 4 meters.

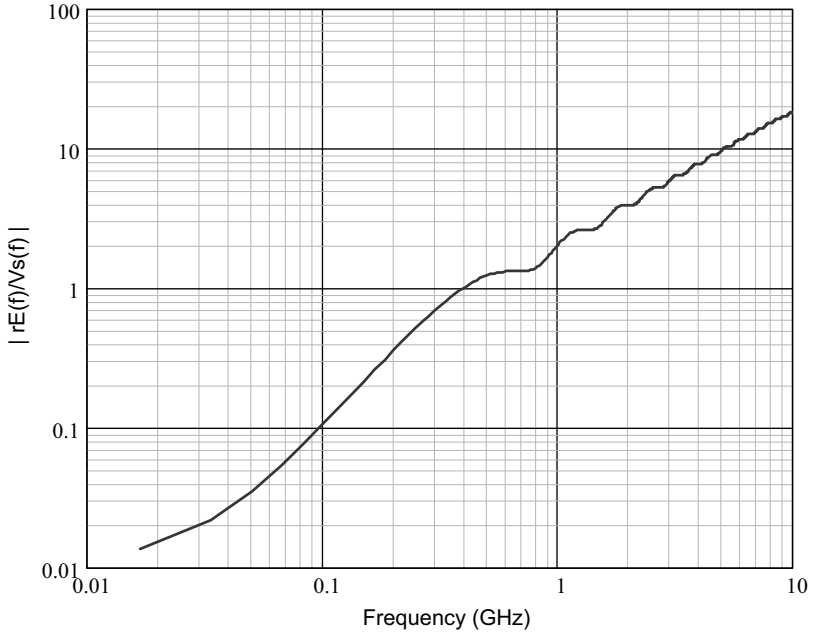

Figure 21. Plot of the field transfer function magnitude $|T_{IRA}| = |rE^{rad}(f)/V_o(f)|$ for the on-axis field for range r = 4 m.

3.1 An Infinite Plate Scatterer

Perhaps the simplest scattering body is a perfectly conducting, infinite plate located directly in front of the IRA, as shown in Figure 22. Because this scatterer is extended in space, it cannot be viewed as a simple point object. As a consequence, we do not expect that the scattered field back at the IRA source will have a $1/r^2$ amplitude fall-off relative to the radiated field. (Recall that there is a $1/r$ term in the field radiated from the IRA and another 1/r term in the reflection coefficient of Eq.(19).

Using image theory, the scattered field at the IRA that results from a reflection in the conducting plate can be thought of as arising from an *image* of the IRA with its voltage excitation source reversed in polarity, as suggested in Figure 22. Clearly, the EM field launched from this image and propagating toward the real IRA will have a $1/2r$ fall-off, not a $1/r^2$ behavior. Consequently, the reflection coefficient Γ for this plate will be

$$\Gamma = -\frac{1}{2}e^{-jkr}. \qquad (20)$$

When this coefficient is used in Eq.(19) we note that the field will have the proper phase, fall-off with distance, and the required change in amplitude due to a reflection from the perfectly conducting plate.

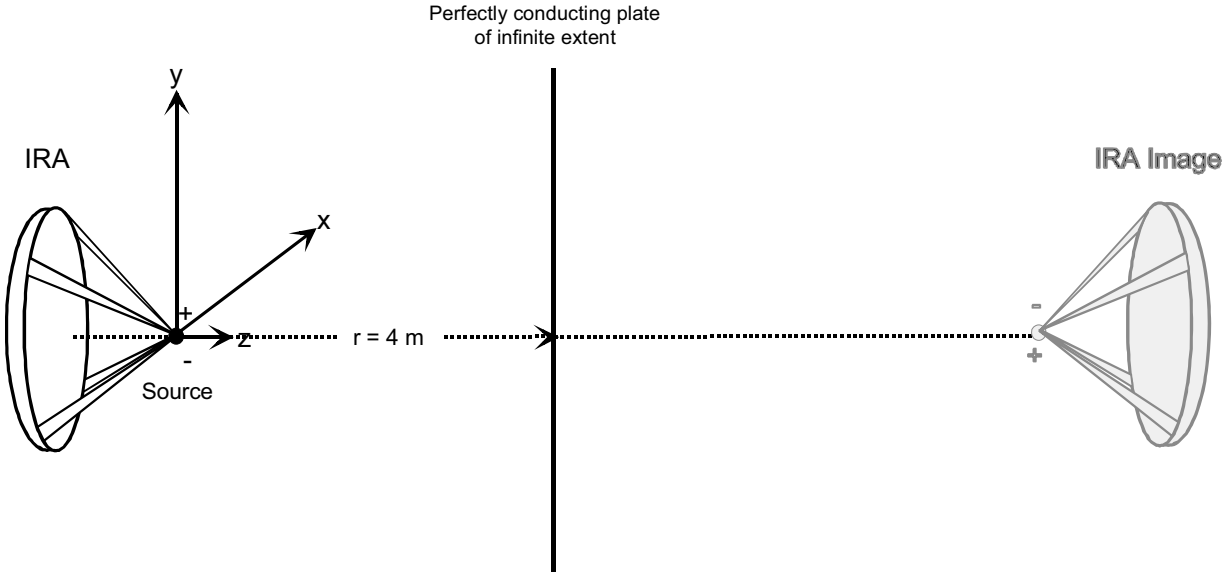

Figure 22. The IRA illuminating an infinite plate, with its image in the plate shown.

For this particular scatterer, a plot of the reflection coefficient Γ as a function of frequency is rather uninteresting, as its amplitude is simply a constant equal to 0.5. Furthermore, the spectral magnitude of the received E-field back at the IRA is just a factor of 2 smaller than that in Figure 20. Additionally, the transient behavior of this received E-field will be that of Figure 19, flipped in sign and scaled by a factor of two. Plots of these fields for the present case are not provided.

Evaluating Eq.(19) for this case with the reflection coefficient in Eq.(20) provides the open-circuit voltage spectrum at the IRA terminals for the wire scatterer. This is shown in Figure 23. The transient response for V_{oc} is presented in Figure 24. Note that the statement is often made that "*the received transient signal of the IRA has the same time history as the incident E-field exciting the antenna*". This statement is not strictly correct, as can be seen by comparing the waveform in Figure 19 (scaled by -0.5) with that of Figure 24. The waveforms are similar, however.

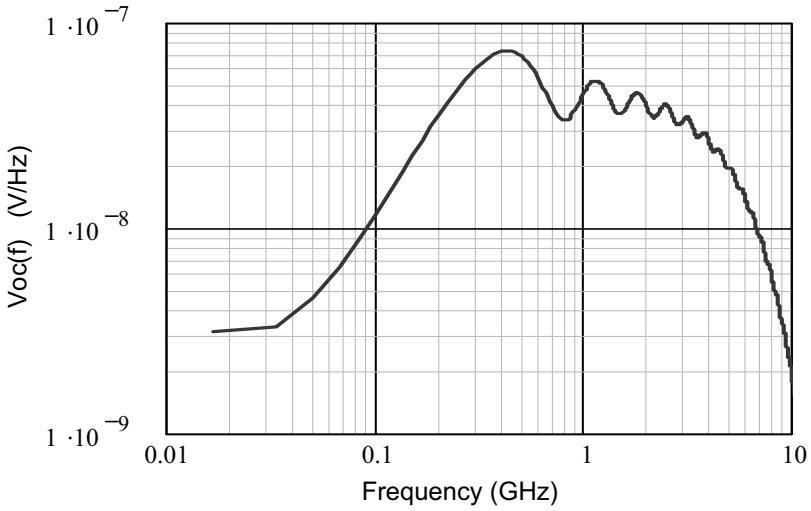

Figure 23. Spectral magnitude of V_{oc} received by the IRA for the infinite plate scatterer at a distance of r= 4 m.

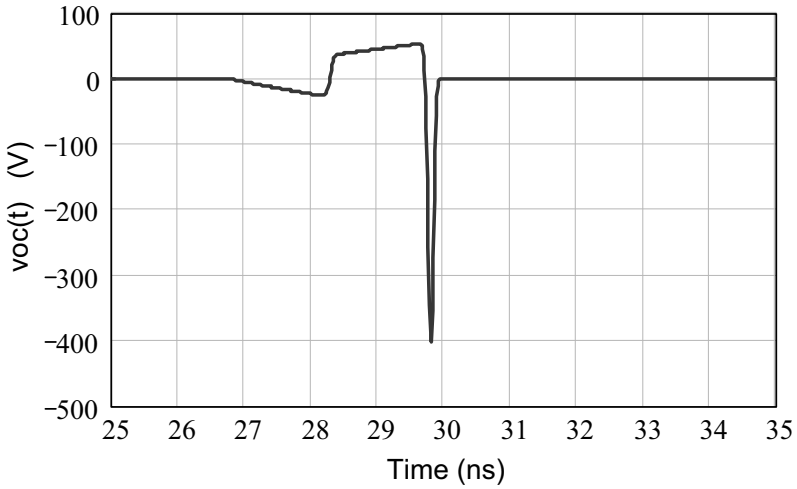

Figure 24. Transient V_{oc} received by the IRA for the infinite plate scatterer at r= 4 m.

3.2 Wire Scatterers

3.2.1 Single Thin Wire, Broadside Incidence

The second example of the scattered field reception of the IRA is provided by examining the response of a thin-wire scatterer located parallel to the radiated E-field from the IRA (in the y-direction shown in Figure 2.) For this calculation, the length of the wire is L = 25 cm, and the radius is a = 0.1 cm. As shown in Figure 25 the center of the wire is located on the boresight direction and the incident field is tangential to the wire.

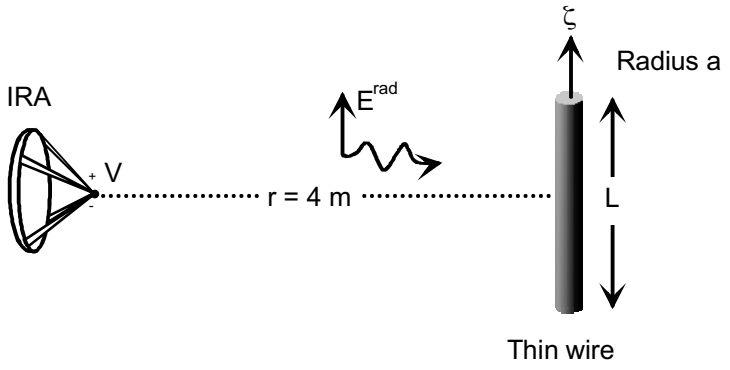

Figure 25. A thin-wire scatterer illuminated by the IRA.

To determine the scattering coefficient $\Gamma(r, f)$ for this wire, an integral equation approach is used [15]. In this method, the following equation is developed for the unknown current $I(\zeta)$ flowing in the wire, which is induced by the incident field from the IRA:

$$-j\omega\varepsilon_o E_\zeta^{rad}(\zeta) = \left[\frac{d^2}{d\zeta^2} + k^2\right] \int_{\text{wire}} I(\zeta') \frac{e^{-jkR}}{4\pi R} d\zeta' \quad , \tag{21}$$

where the distance R is given by

$$R = \sqrt{(\zeta - \zeta')^2 + a^2} \ .$$

The solution for the current in Eq.(21) can be determined using the method of moments described by Harrington [16], and once this current is known, the scattered E-field back at the IRA can be obtained by integrating over the wire current distribution as [14].

$$E_\zeta^{ex} \approx \frac{-jkZ_c}{4\pi r} \frac{e^{-jkr}}{r} \int_{-L/2}^{L/2} I(\zeta') e^{-jk\zeta'} d\zeta' . \tag{22}$$

The scattering coefficient is then calculated as

$$\Gamma(f) = \frac{E_y^{rad}}{E_y^{ex}} = \frac{\dfrac{-jkZ_c}{4\pi r}\dfrac{e^{-jkr}}{r}\displaystyle\int_{-L/2}^{L/2} I(\zeta')e^{-jk\zeta'}d\zeta'}{E_y^{ex}} \tag{23}$$

and this is used in Eq.(19) to compute the open circuit voltage spectrum of the received signal at the IRA terminals.

Before proceeding with the illustration of the wire responses, however, it is useful to check the numerical solution used for the wire scatterer, which was implemented in MathCAD. For a thin wire of length L and radius $a = L/148.4$, Harrington [16] computes and plots the normalized backscatter cross-section for broadside incidence as

$$\sigma = 4\pi r^2 \frac{\left|E^{ex}\right|^2}{\left|E^{rad}\right|^2}. \tag{24}$$

Figure 26 provides a comparison of this scattering cross-section for this particular wire using the present MathCAD computational model (a) and the numerical values reported by Harrington (b). Note that these are plots of normalized cross-sections σ/λ^2 and are plotted as a function of normalized frequency $L/\lambda = Lf/c$. As may be seen from these plots, the results are identical.

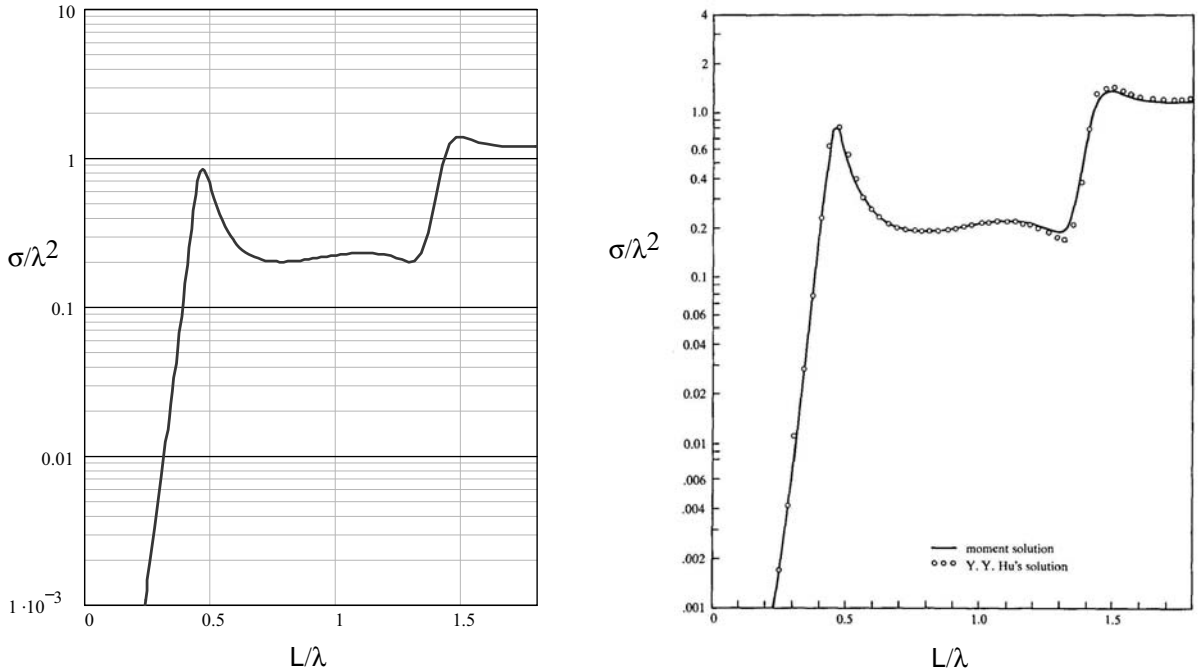

(a) Present calculation (b) Harrington [16].

Figure 26. Comparison of the normalized backscatter cross-section for the wire for broadside incidence.

From the integral equation solution for the thin-wire current, the scattered field has been calculated and the scattering coefficient $\Gamma(r,f) = E_y^{ex} / E_Y^{rad}$ is plotted in Figure 27. Multiplying this scattering coefficient by the radiated field spectrum in Figure 20 yields the spectrum of the returned field that excites the IRA in the receiving mode. This spectrum is shown in Figure 28. Taking the Fourier transform of this latter spectrum provides the transient E^{ex} field that excites the IRA. This is shown in Figure 29.

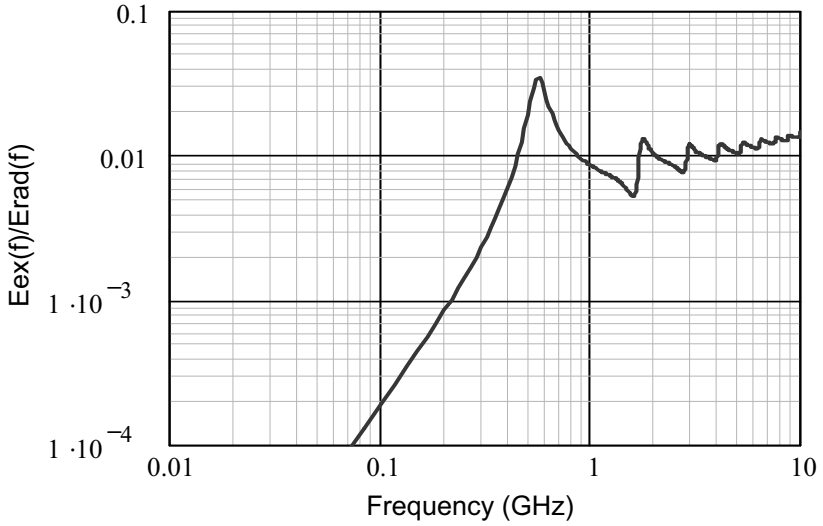

Figure 27. Plot of the magnitude of the scattering coefficient Γ(*f,r*) for the thin wire at a range of 4 meters.

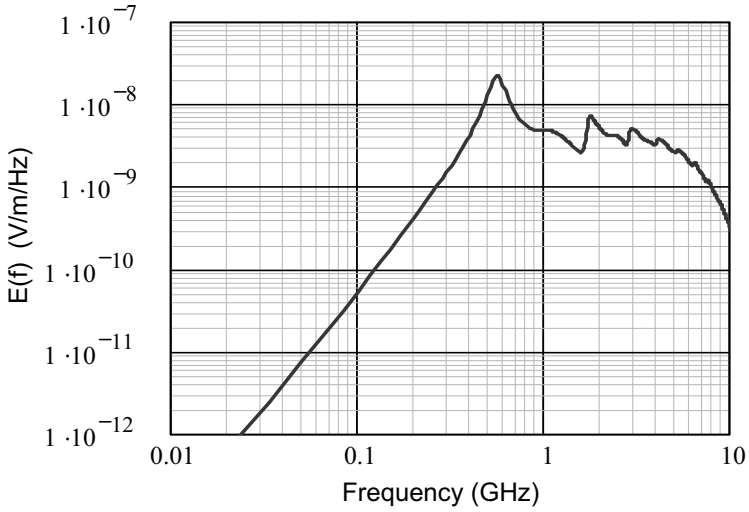

Figure 28. Plot of the magnitude of the E-field scattered from the wire and exciting the IRA in receive mode.

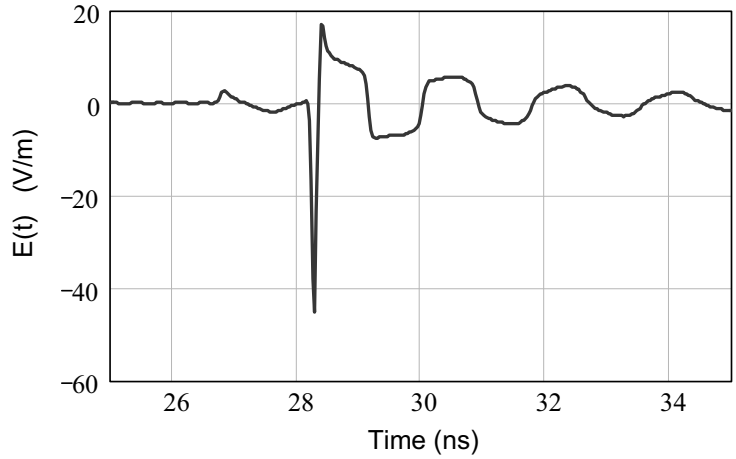

Figure 29. Transient response of the E^{ex} field received at the IRA for the thin-wire scatterer at r= 4 m.

Evaluating Eq.(19) with all of the appropriate spectra provides the open-circuit voltage spectrum at the IRA terminals for the wire scatterer. This is shown in Figure 30 and the corresponding transient response for the IRA V_{oc} is presented in Figure 31.

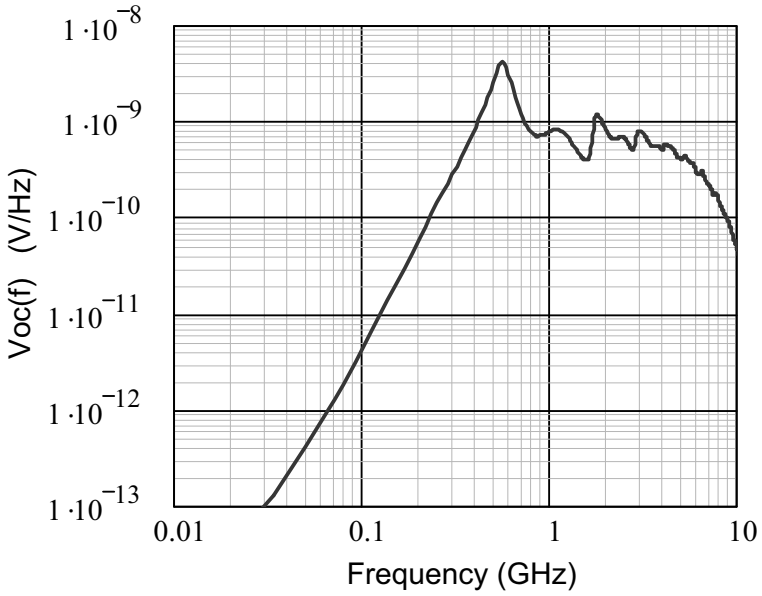

Figure 30. Spectral magnitude of V_{oc} received by the IRA for the thin-wire scatterer at r= 4 m.

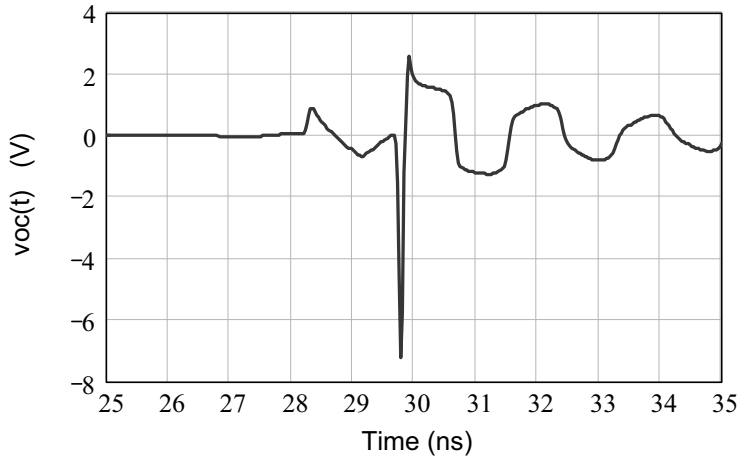

Figure 31. Transient V_{oc} received by the IRA for the thin-wire scatterer at r= 4 m.

As a final check of the numerical solution for the scattering, the Numerical Electromagnetics Code (NEC) [17] was used to solve the integral equation (21) and compute the scattered field (22). The resulting V_{oc} at the IRA is shown in Figure 32, and this is virtually identical with the MathCAD results of Figure 31

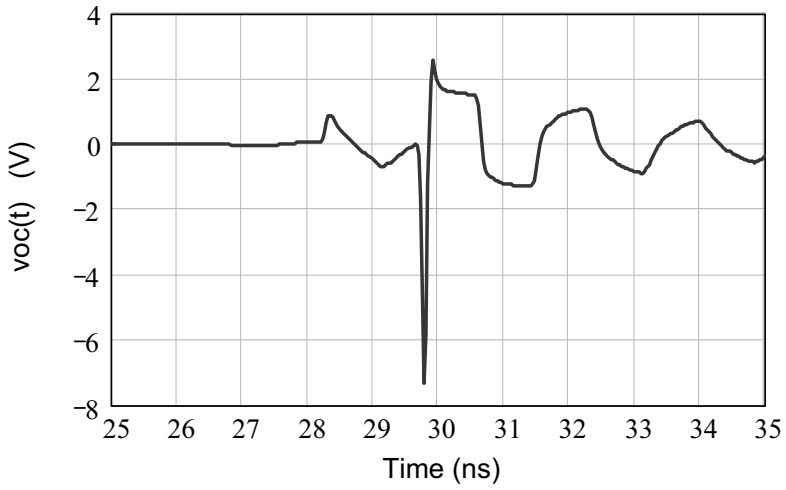

Figure 32. Transient V_{oc} received by the IRA using calculations from the Numerical Electromagnetics Code (NEC).

3.2.2 Single Thin Wire, Varying Angle of Incidence

Another interesting thin-wire case is when the thin wire is inclined relative to the boresight direction from the IRA. Considering the wire to lie in the *y-z* plane and inclined by an angle θ, as shown in Figure 33, the received V_{oc} waveforms and spectral densities have been computed for different angles of illumination, ranging from the wire being illuminated broadside ($\theta = 0^o$, as in the previous section) to nearly end-on incidence ($\theta = 75^o$).

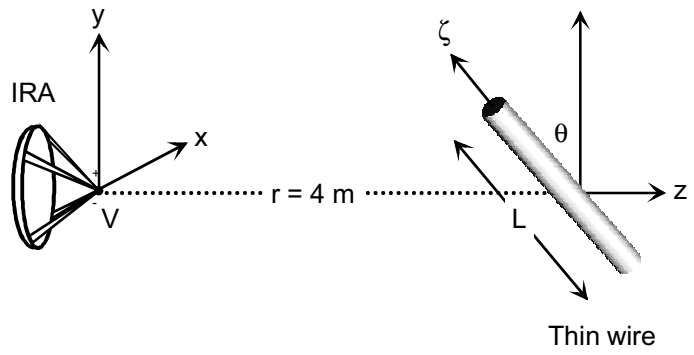

Figure 33. Geometry of the thin-wire scatterer at an inclined angle, θ.

Figure 34 presents the transient responses for the varying angles of incidence. It is noted that in the broadside direction ($\theta = 0^o$), the V_{oc} waveform has the large impulse-like spike in the response. For other angles of incidence, this spike is largely missing. Figure 35 presents the spectral magnitudes for V_{oc} for these cases.

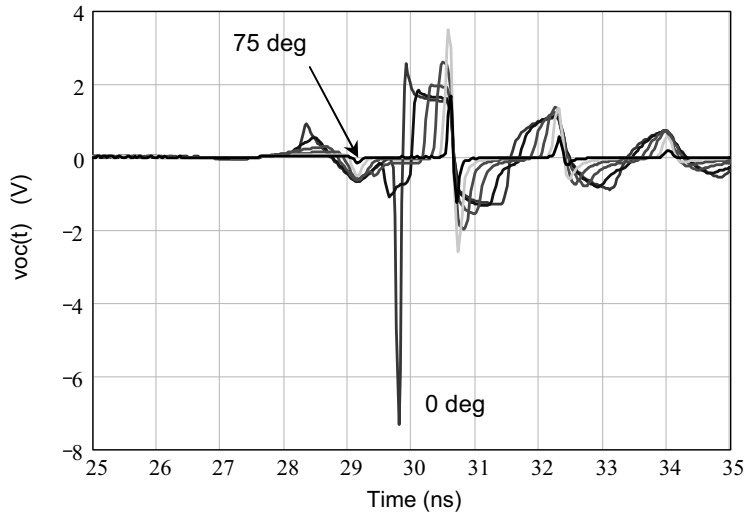

Figure 34. Plot of the transient V_{oc} response for the thin-wire scatterer of length L = 0.25 m for different angles of incidence.

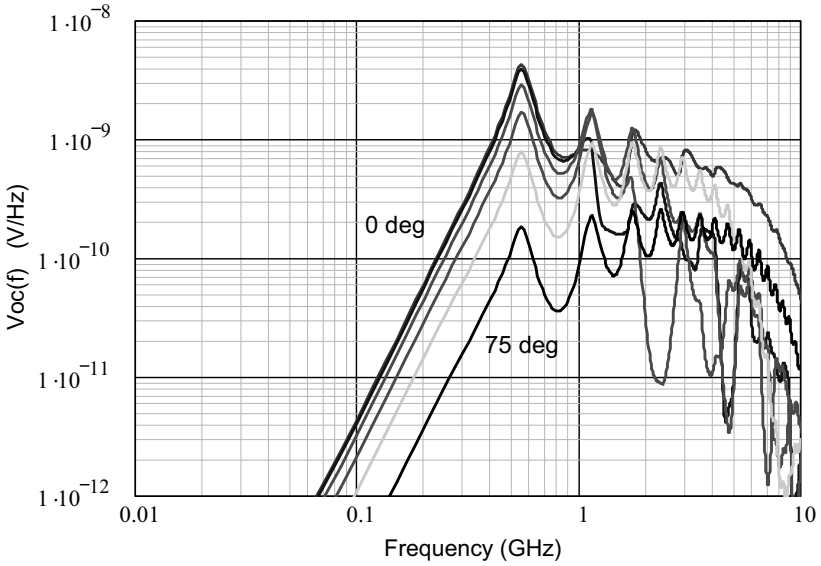

Figure 35. Plot of the spectral magnitude $|V_{oc}(f)|$ for the thin-wire scatterer of length L = 0.25 m for different angles of incidence.

3.2.3 Multiple Wires

It is also of interest to examine the effects of having a scattering target consisting of two thin wires. Consider the case of two identical length wires (L = 25 cm, a = 0.1 cm), separated by a distance d, which is varied.

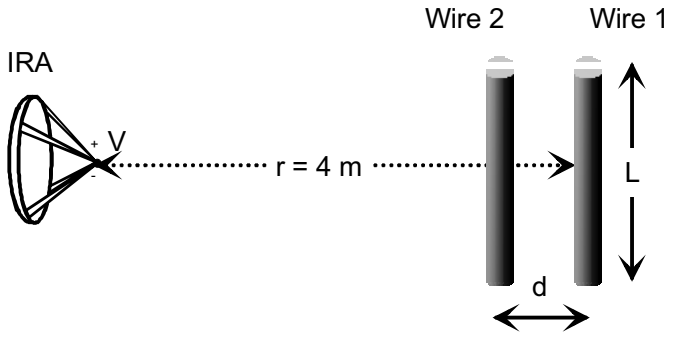

Figure 36. Scatterer configuration of two equal length wires, separated by a distance *d*.

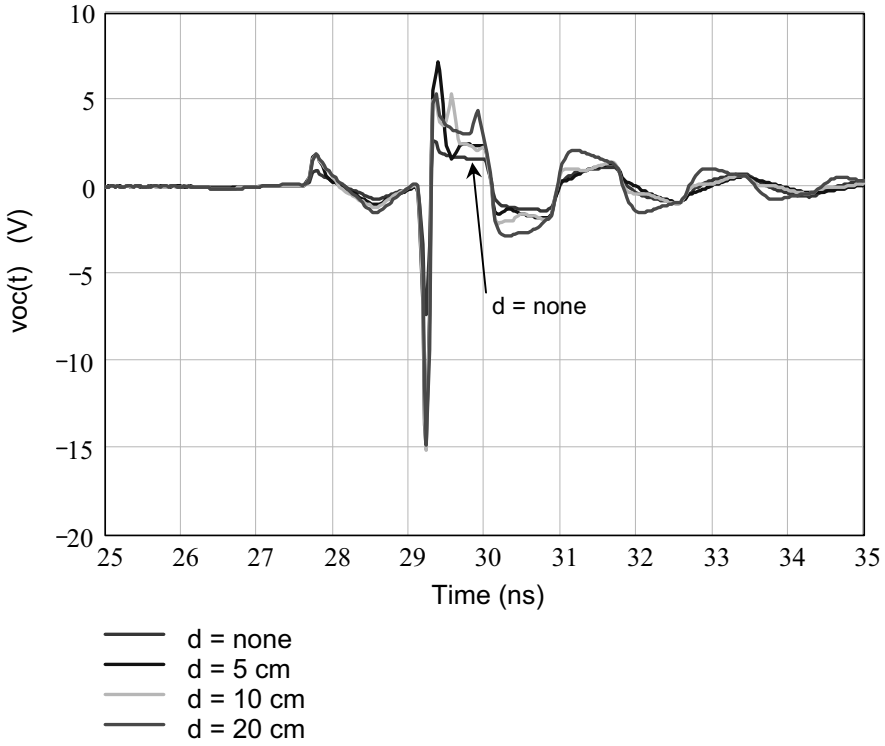

Figure 37. Transient V_{oc} responses for the two-wire scatterer of Figure 36, for different values of *d*. (The case of *d* = none refers to wire 2 being absent.)

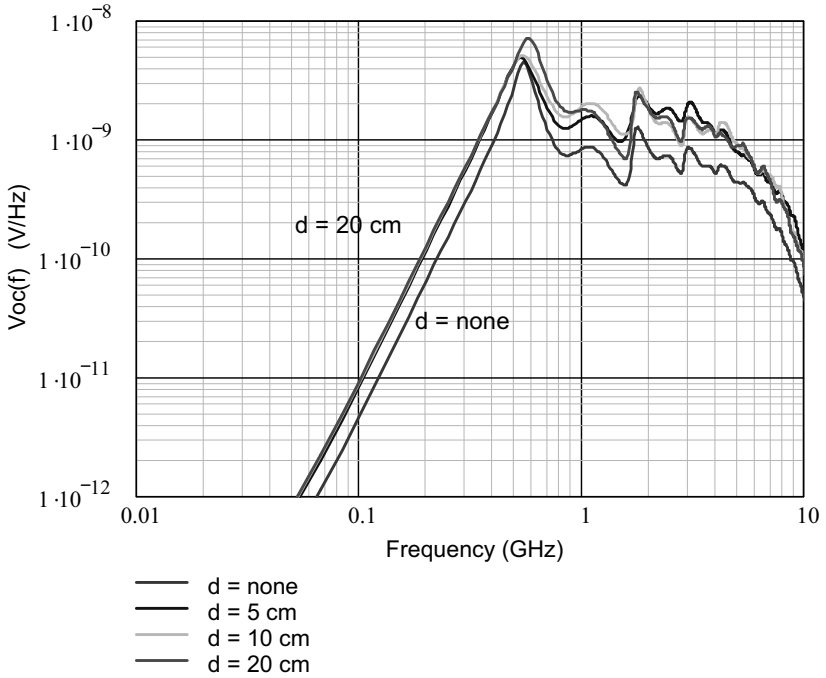

Figure 38. Spectral magnitudes of V_{oc} for the two-wire scatterer of Figure 36, for different values of *d*.

In these plots, it is clear that the returned signal is greater for two wires than for a single wire (the red curve.) While both wires have the same length and the same resonant frequency if the wires are isolated and in free space, there is a mutual interaction between the two when they are close together. This interaction increases as the distance between the two decreases. The amplitudes for a single wire and 2 widely separated wires are roughly a factor of two different.

A variation of the previous two-wire geometry is shown in Figure 39, where the wires have a different lengths, but the distance between the is constant. In the following calculations, L_1 = 25 cm as before, d = 10 cm, and L_2 is variable. As before, the wire radii are equal to 0.1 cm.

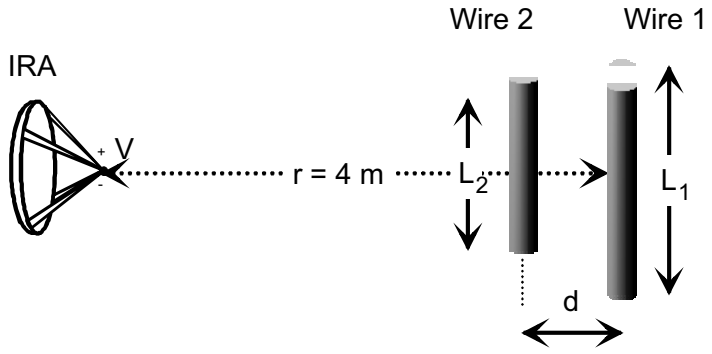

Figure 39. Scatterer configuration of two different length wires, separated by a constant distance *d*.

Figure 40 shows the transient responses for this wire configuration, as the length of wire 2 varies from 25 cm to 10 cm. Figure 41 shows the corresponding spectral magnitudes.

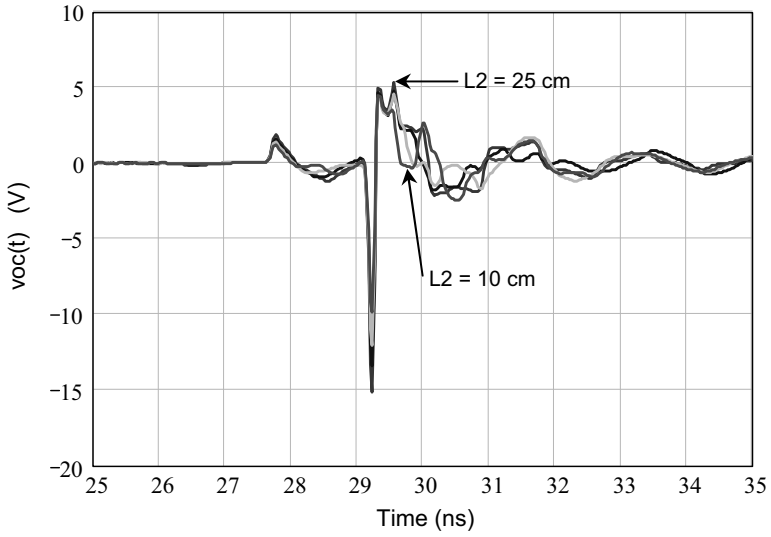

Figure 40. Transient V_{oc} responses for the two-wire scatterer of Figure 39, for different values of wire 2 length, L_2 (d = 10 cm).

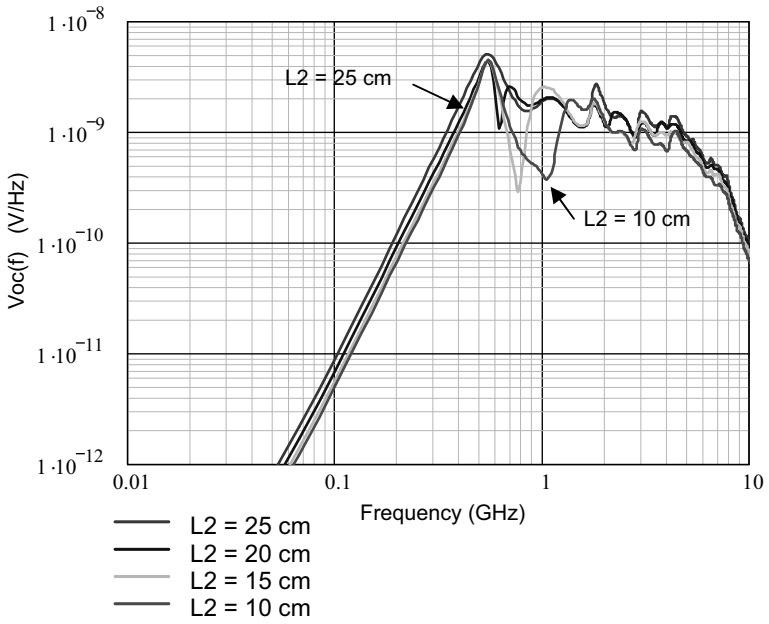

Figure 41. Spectral magnitude of V_{oc} for the two-wire scatterer of Figure 39, for different values of wire 2 length, L_2 (d = 10 cm).

3.3 Spherical Scatterer

Because the EM scattering can be calculated analytically, a spherical scatter is commonly used as a test case for checking computations and for calibrating test ranges. A possible geometry for the IRA measurements is shown in Figure 42, where the sphere has a radius of a = 5 cm. The sphere is located with its center at a distance of 4 meters from the IRA.

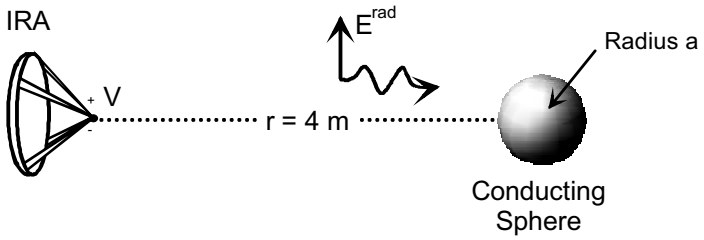

Figure 42. Scattering geometry for a sphere of radius *a*.

To compute the scattering coefficient for the sphere, the classical Mie series for the scattering is used [18]. For an incident E-field propagating in the z direction and with a polarization in the x direction, as portrayed in Figure 43, the q component of the scattered E-field at a far-field observation point defined by the parameters (r, θ and ϕ) can be written as an infinite sum

$$E_{\theta}^{sca} = \frac{jE^{rad}}{kr} e^{-jkr} \cos\phi \sum_{n=1}^{\infty} j^n \left[b_n \sin\theta P_n^{1\prime}(\cos\theta) - c_n \frac{P_n^1(\cos\theta)}{\sin\theta} \right] \tag{25}$$

Where the terms a_n and b_n are given by

$$b_n = -\frac{j^{-n}(2n+1)}{n(n+1)} \frac{j_n'(ka)}{h_n^{(2)\prime}(ka)} \tag{26a}$$

$$c_n = -\frac{j^{-n}(2n+1)}{n(n+1)} \frac{j_n(ka)}{h_n^{(2)}(ka)}; \tag{26b}$$

In these expressions above, $j_n(ka)$ and $h_n^{(2)}(ka)$ are spherical Bessel and Hankel functions, and $P_n^1(\cos\theta)$ is the associated Legendre polynomial.

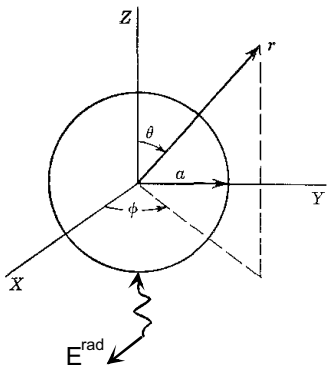

Figure 43. Illustration of a sphere illuminated by a *x*-polarized plane-wave E-field propagating in the *z* direction. (From [18].)

In examining the geometry of Figure 42, we note that the scattered field back to the IRA is given by

$$E_x^{sca} = E^{ex} = E_\theta\big|_{\substack{\theta=\pi \\ \phi=\pi}} . \tag{27}$$

Evaluating Eq.(25) for $\theta = \pi$ and $\phi = \pi$ and r = 4 m, thus provides the scattered field at the IRA and the reflection coefficient for the sphere. To check the calculation of the sphere scattering, Harrington [18] has provided a plot of the scattering cross-section defined in Eq.(24) normalized by the wavelength squared. A comparison of his results with those obtained by the present MathCAD calculation is shown in Figure 44. The agreement is again excellent.

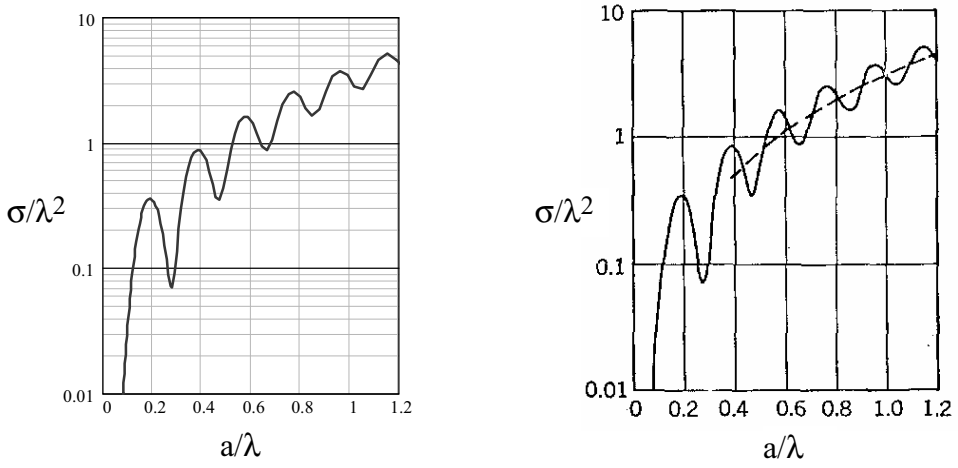

(a) Present calculation (b) Harrington[18].

Figure 44. Comparison of the normalized backscatter cross-section for the sphere.

The following plots present scattering data for the 5 cm sphere. This is in the same format as done for the single thin-wire in Section 3.2.1.

Figure 45 shows the plot of the magnitude of the scattering coefficient Γ(*r, f*) for the sphere at a range of 4 meters and from this, the spectrum of the received E-field at the IRA is calculated. This spectrum is presented in Figure 46. The corresponding transient response of this scattered field at the IRA is shown in Figure 47.

Figure 48 plots the spectral magnitude of V_{oc} induced in the IRA for the spherical scatterer and the corresponding transient response is shown in Figure 49.

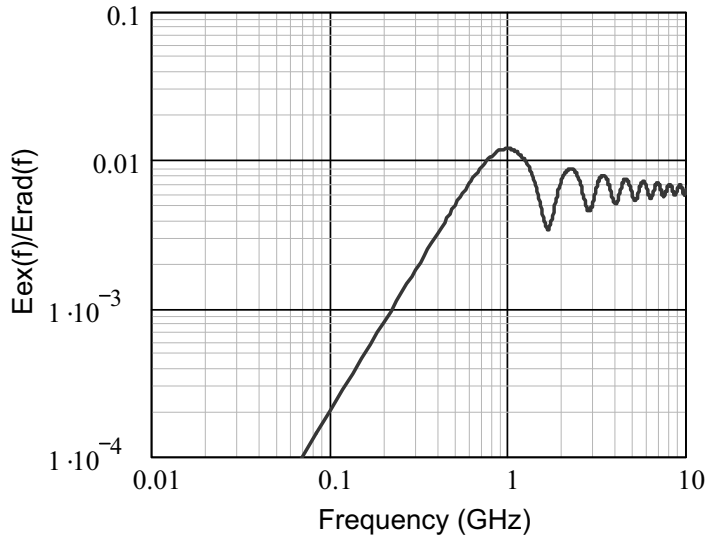

Figure 45. Plot of the magnitude of the scattering coefficient Γ*(r, f)* for the spherical scatterer with radius of 5 cm.

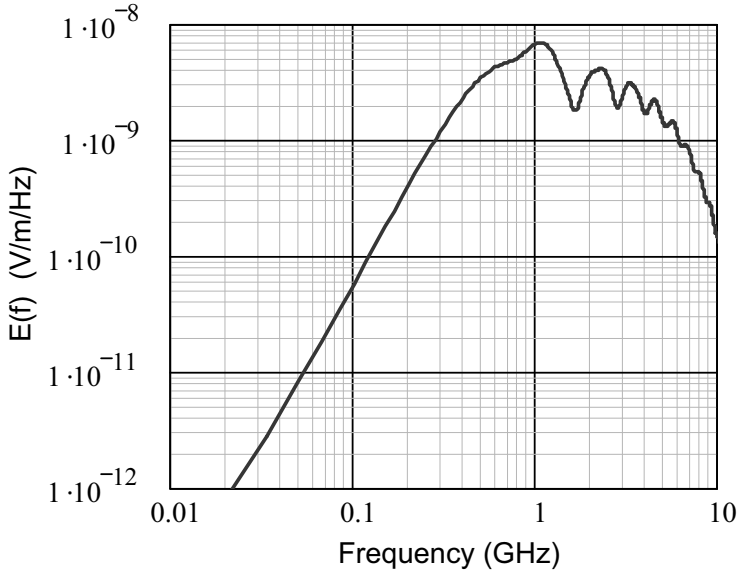

Figure 46. Plot of the magnitude of the E-field scattered from the sphere and observed at the IRA.

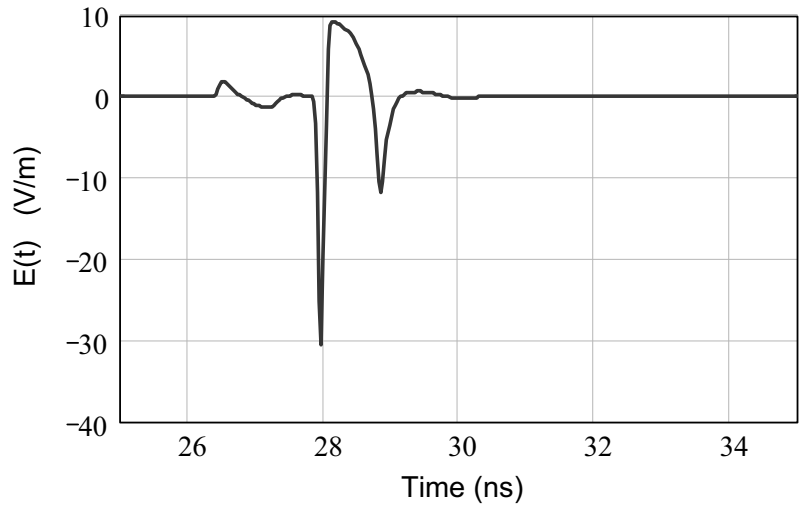

Figure 47. Transient response of the E^{ex} field received at the IRA for the spherical scatterer of radius 5 cm.

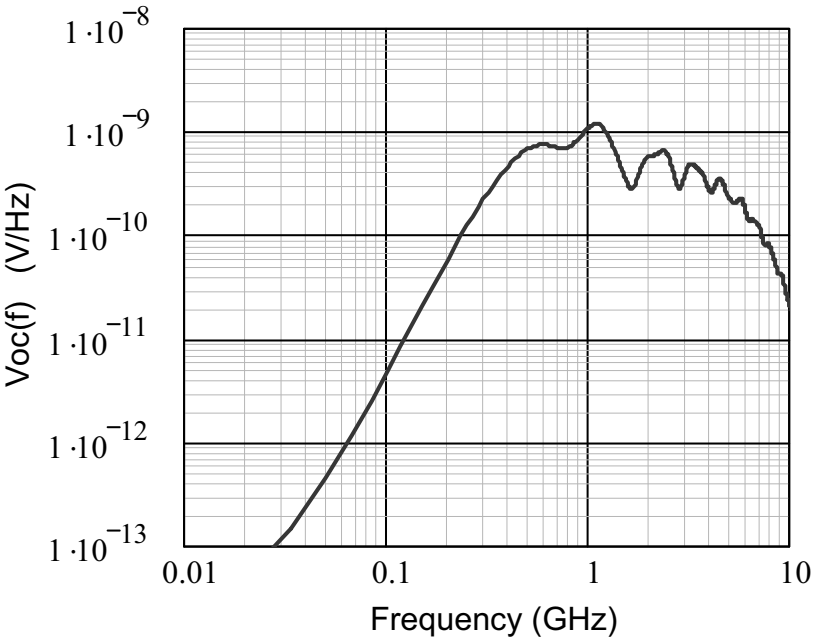

Figure 48. Spectral magnitude of V_{oc} received by the IRA for the spherical scatterer.

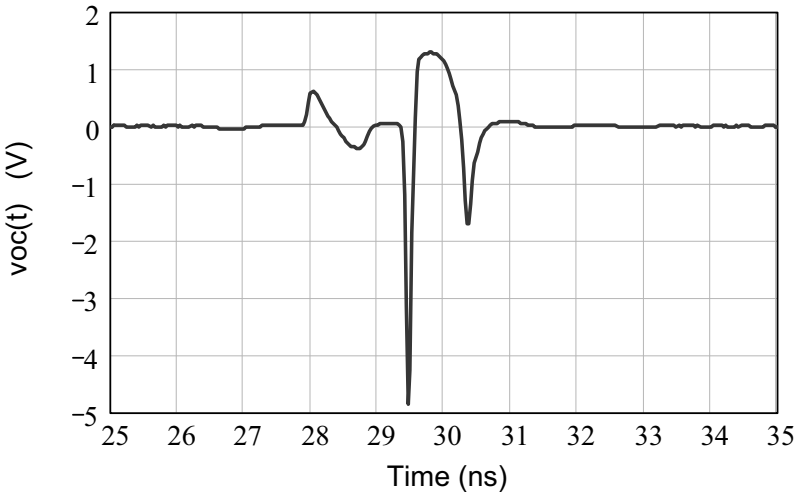

Figure 49. Transient V_{oc} received by the IRA for the spherical scatterer of radius 5 cm.

It is useful to consider the scattering responses for several spheres of different radii. To this end spheres with radii varying from 1 cm to 20 cm were analyzed and the results are presented below. Figure 50 plots the transient V_{oc} for the IRA for different sphere radii, and the spectral magnitudes are given in Figure 51. Note that as the sphere gets larger, so does the response, as is expected.

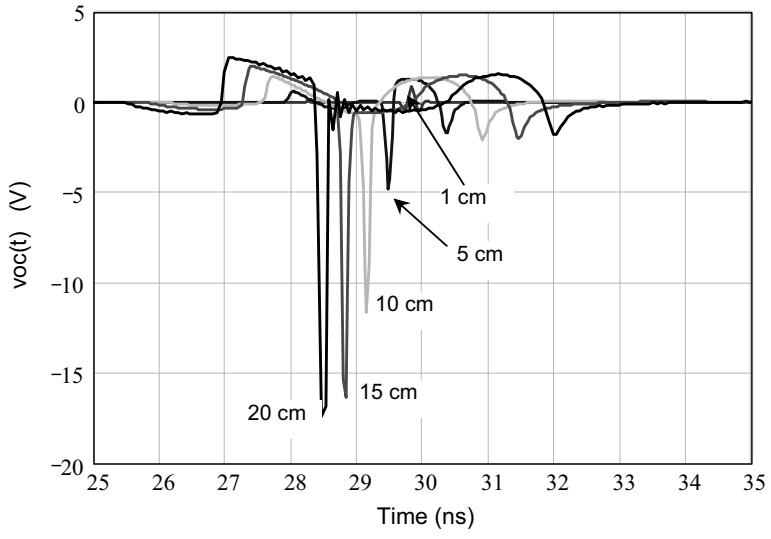

Figure 50. Plot of the transient V_{oc} at the IRA for a sphere at range r =4 m with a variable radius a.

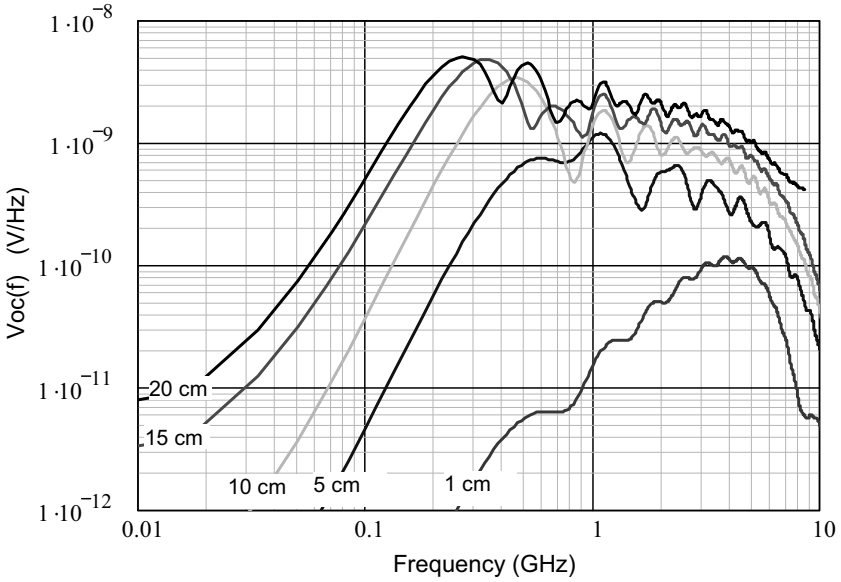

Figure 51. Plot of the spectral magnitude for $|V_{oc}|$ at the IRA for a sphere at range r =4 m with a variable radius a.

3.4 Box Scatterer

Another canonical scatterer is a small rectangular conducting box having a side dimension a. This is shown in Figure 52. For this calculation, the box was modeled using the surface patch capacity in NEC [17].

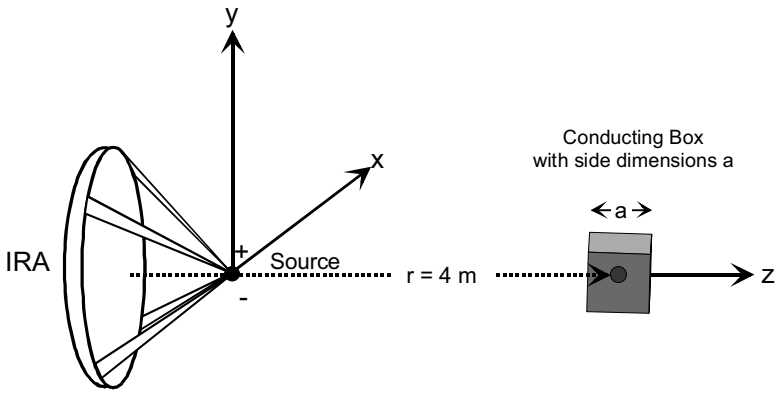

Figure 52. The IRA illuminating a small rectangular cube of side dimension *a*.

Figure 53 presents the scattering coefficient Γ for a 10 cm box at a distance of 4 meters. Initially, its scattering behavior is similar to that of the sphere (in Figure 45), but after a few oscillations at high frequencies, the scattering appears to be continuing to grow, while that of the sphere oscillates around a limit value. Most notable in this curve are the resonances at the higher frequencies. A close examination of these spikes shows that they are occurring at the internal resonant frequencies of the box and are an unwanted artifact in the numerical solution of NEC. This is a well-known phenomenon and its thorough discussion is beyond the scope of the present note.

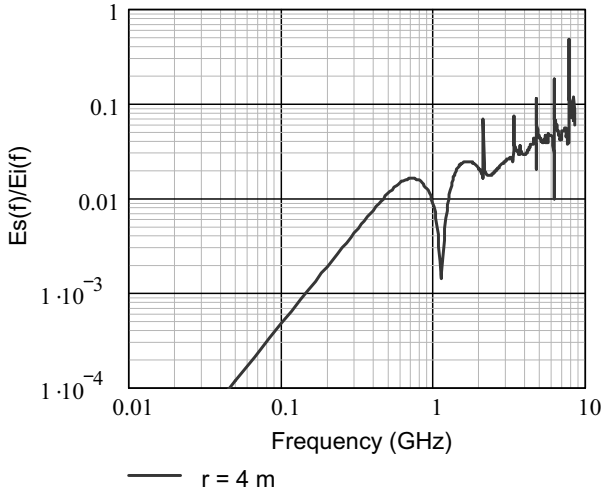

Figure 53. Plot of the magnitude of the scattering coefficient Γ*(r, f)* for the box with *a* = 10 cm.

Figure 54a illustrates the range of transient V_{oc} responses for three different box sizes at the range of 4 m from the IRA. Note that the effects of the numerical "noise" introduced in the NEC solution by the internal box resonances is most pronounced in the large, 20 cm box. Nevertheless, a rough indication of the peak values of the expected received voltage is provided. In this plot, the details of the induced voltage for the small 5 cm box is difficult to see, so this waveform is re-plotted in part *b* of the figure.

The Fourier transform of these transient waveforms provides the spectra of the V_{oc}, and there are provided in Figure 55.

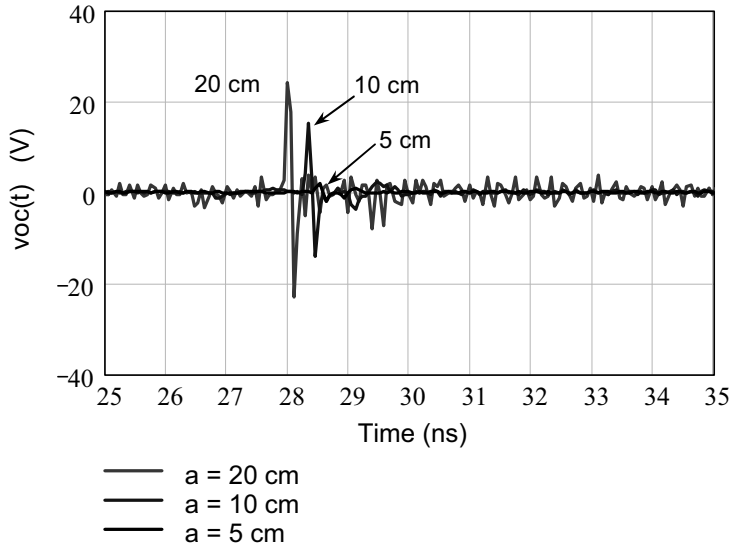

(a) The V_{oc} waveforms for three box sizes.

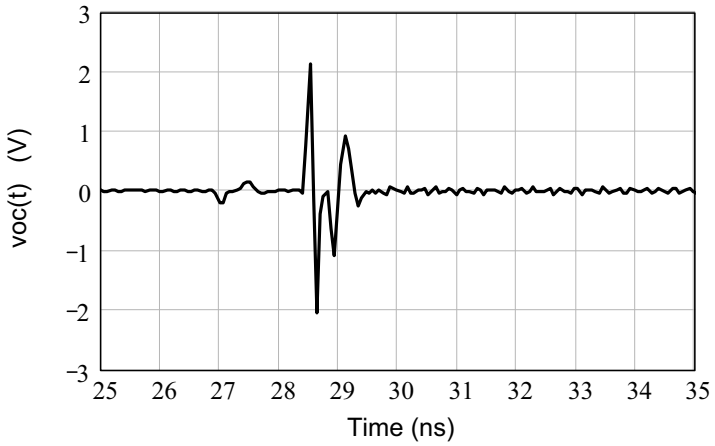

(b) V_{oc} waveform for the 5 cm box.

Figure 54. Plot of the transient V_{oc} at the IRA for different boxes at range r =4 m.

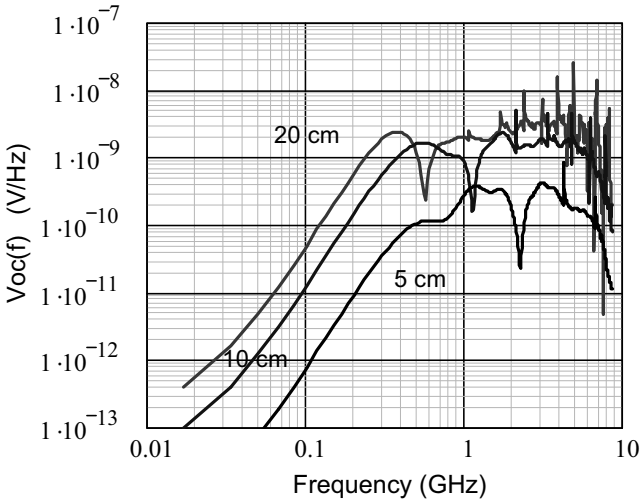

Figure 55. Plot of the spectral magnitude for $|V_{oc}|$ at the IRA for different box scatterers.

4. Summary

Using a simple model for calculating the radiated EM field from a 46 cm IRA, the backscattered field for a number of canonical scatterers at a distance of 4 meters from the antenna has been calculated. These backscattered fields are assumed to be received by the same IRA and result an open circuit voltage response of the antenna. Details of the spectral and transient responses for these induced voltages are examined, and for the transient responses, the approximate peak values of the impulse-like contribution to the waveforms are summarized in Table 1.

Table 1. Summary of peak values of V_{oc} for different scattering bodies.

Scatterer	Approximate Peak V_{OC} (V)
Infinite Plate	400
Thin wire (25 cm)	7
Two thin wires (25 cm)	14
Sphere (5 cm radius)	5
Sphere (20 cm radius)	20
Box (5 cm side)	2
Box (20 cm side)	22

5. References

1. R. H. DuHamel, M. B. Armstrong, J. J. Campbell, W. R. Jones, and W. F. Pedler, Frequency Independent Conical Feeds for Lens and Reflectors, *Proceedings of the IEEE APS Symposium*, 1968.

2. *Baum, C. E., "Radiation of Impulse-Like Transient Fields," Sensor and Simulation Note 321*, 25 November 1989.

3. Baum, C. E., and E.G. Farr, "Impulse Radiating Antennas," in **Ultra-Wideband Short Pulse Electromagnetics**, edited by H. L. Bertoni et al., pp 139-147, Plenum Press, NY 1993.

4. Giri, D. V., "Selected Applications of Hyperband Systems", to be presented at AMEREM 2006, Albuquerque, NM , July 7-14, 2006.

5. Smith, I. D., D. W. Morton, D. V. Giri, H. Lackner, C. E. Baum, J. R. Marek, " Design, Fabrication and Testing of a Paraboloidal Reflector Antenna and Pulser System for Impulse-Like Waveforms", *Proceedings of the Tenth IEEE International Pulsed Power Conference*, Albuquerque, NM, July 3-6, 1995, Vol. 1, pp 56-64. Also in *IEEE Trans Plasma Science*, April 1997, pp 318-326.

6. Farr, E., “Development of a Reflector IRA and a Solid Dielectric Lens IRA, *Sensor and Simulation Note 396*, April 1996.

7. Baum, C. E., “Configurations of TEM Feed for an IRA”, *Sensor and Simulation Note 327*, 27 April 1991.

8. Giri, D. V., **High-Power Electromagnetic Radiators: Nonlethal Weapons and Other Applications**, Harvard University Press, November 2004.

9. Giri, D. V., . M. Lehr, W. D. Prather, C. E. Baum, and R. J. Torres, “Intermediate and Far Fields of a Reflector Antenna Energized by a Hydrogen Spark-Gap Switched Pulser”, *IEEE Trans. Plasma Science*, Oct. 2000.

10. Mikheev, Oleg V., et. al, “New Method for Calculating Pulse Radiation from an Antenna with a Reflector”, *IEEE Trans. EMC*, February 1997.

11. Farr, E., “Optimizing the Feed Impedance of Impulse Radiating Antennas, Part I: Reflector IRAs”, *Sensor and Simulation Note 354*, January 1993.

12. Tesche, F. M., “Swiss Impulse Radiating Antenna (SWIRA) Characterization”, Report for Contract 4500314446 for the HPEM-Laboratory, Spiez, Switzerland, August 8, 2005.

13. Plonsey, R. and R. E. Collin, **Principles and Applications of Electromagnetic Fields**, McGraw-Hill, New York, 1961

14. Tesche, F. M., M. Ianoz, and T. Karlsson, **EMC Analysis Methods and Computational Models**, John Wiley & Sons, New York, 1996

15. Mei, K. K., "On the Integral Equations of Thin Wire Antennas", *IEEE Trans. AP.,* Vol. AP-13, No.3, May 1965, pp. 374-378.

16. Harrington, R. F., **Field Computation by Moment Methods**, reprinted by the author, Syracuse University, Syracuse, NY, 1968.

17. Burke, G. J., and A. J. Poggio, "Numerical Electromagnetic Code (NEC) - Method of Moments," NOSC Tech. Doc. 116, Naval Ocean Systems Center, San Diego, CA, January 1980.

18. Harrington, R. F., **Time Harmonic Electromagnetic Fields**, McGraw Hill, New York, 1961.